



BEng Mechanical Engineering 4 Project

The Design of a Small Wind Machine for the Television and Film Industry

Meagan Rutledge

Supervisor: Dr John Chick

Second Marker: Dr Jane Blackford

April 2019

Personal Statement

This was an original project to design a small wind machine for the prop and special effects production company, Artem. The company supplied the brief and the major requirements, but within this I was allowed a large scope of design freedom. This required my own judgement on the most important requirements through research and discussion with the company.

The main wind machine design, a fan, required a combination of the skills and theory I have gained throughout my university degree. Notably, almost all of the modules I have taken this year: Fluid Mechanics, Thermodynamic, Dynamics and Digital Manufacture were all very useful in the understanding and execution of the project. Even Project Management helped with project planning and producing a Gantt Chart. It seemed a fitting project to hone the skills I've gained over university.

I found the project challenging, but stimulating as it required a high level of understanding for a fairly broad topic in a short space of time. Although I would have liked to test the machine in order to more confidently analyse the success of the design, I feel I have achieved a significant amount over the course of this project, from a sound understanding of the theory to the practical design of the machine.

The project gave me insight into real-world designing work. Especially for a company like Artem which commonly employs freelancers, I was essentially working as one, giving me insight into what that would entail. This gave me invaluable experience in interacting with others on a professional level and understanding possible delays which can arise when coordinating with a group of people, especially when working from across the country, and communicating mainly through phone and email. Unlike with most projects at university, I was not just relying on my own organisation, but that of a company which has many other projects going on simultaneously.

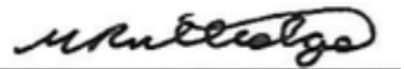
This project was an interesting balance between academic and practical engineering and highlighted how the optimal engineering is rarely adopted due to time and cost constraints. Interestingly, this was a repeated theme throughout my reading for this project. Especially for fans which can be produced quickly and are a trusted piece of equipment there is reluctance by companies to spend too much time simulating and optimising the design when it is assumed they will work ‘well enough’. This project highlighted how cost and ease of manufacturing take precedence.

I approached this project predominantly from an academic viewpoint, however quickly realised I had to start thinking more practically. In turn, my academic approach enabled me to intuitively understand whether seemingly practical solutions were technically viable. Having researched the subject thoroughly, I then applied my findings to the design solution. Dr John Chick, my supervisor, helped me focus my attention in the right direction with weekly meetings where he would question my methods and remind me of any factors I may have overlooked. I also had help with my approach to the design manufacturability from the staff at Artem, as well as at Edinburgh, most notably Chris

Sturgeon and Frank Mill who guided my use of fixtures and Solid Edge, respectively.

All of the work is produced by myself, unless specifically cited and stated otherwise. Clearly conversations with those mentioned above helped me develop some of my ideas, the presentation and application of them was my work.

Meagan Rutledge

A handwritten signature in black ink, appearing to read "Meagan Rutledge". It is written in a cursive style with a horizontal line underneath it.

27.04.2019

Abstract

The Design of a Small Wind Machine for the Television and Film Industry

Meagan Rutledge

April 2019

Wind machines are commonly used in the entertainment industry to evoke atmosphere in fashion shoots, films and adverts. The special effects production company Artem produces these machines for such uses. They required a modernised and improved model of their smallest machine using a variable speed 240v electric motor. The wind machine was subject to a number of constraints. The most important of these were: size, production of wind speeds of 40 mph, pan and tilt mechanisms, minimum cost and ease of manufacturing.

A wind machine consists of a main fan design, motor, protective guards, mount and a stand. Literature pertinent to fans were extensively researched in order to inform the design. An axial fan was concluded to be the most appropriate fan type for a wind machine due to air volume characteristics. Fundamental principles of wind machine design were investigated through mathematical analysis. From this initial research the most important parameters for aerodynamic performance were identified as blade design, hub-to-tip ratio, tip clearance, operating range, and the use of an inlet bell and stators.

Effort was taken to avoid over-engineering of the design for the context of the entertainment industry. A simple set of design rules were constructed to develop a design of optimal aerodynamic performance while minimising cost. This included: a tip clearance of 1% of the impeller diameter; rotor-stator clearance of 10% of the impeller diameter; inlet bell of elliptical profile with dimension ratios of 2.67; materials of low roughness and use of aerofoil blades.

The project involved vibrational analysis using Solid Edge® to assess the risk of resonance. The fan housing and the U-stand were both modelled and natural frequencies of 486Hz and 116Hz were predicted respectively. These are both significantly larger than the forcing frequency of 50Hz the motor. The risk of resonance from these structures is low.

CFD simulations using ANSYS® predicted aeroacoustics and the flow field through various inlet bells. The inclusion of an inlet bell significantly improved flow characteristics but a smaller inlet bell than the recommended 14% of the housing diameter was deemed sufficient. This was used to minimise the dimensions of the machine to 762mm. Noise predictions using the Ffowks Williams and Hawkins method with RANS and LES were carried out on the rotor and housing, using mesh sliding method to model the rotation. Issues with meshing and computation ultimately meant that only broadband noise was modelled. This produced a predicted noise power of 84.5dB. This is in-line with axial fans, and suggests good tip clearance and shroud design. However this assessment is limited by the failure of tonal noise predictions, and lack of rotor-stator interaction.

The final design was modelled on Solid Edge and consisted of an aerofoil PAG rotor produced by Hascon ® of 600mm diameter with 9 blades, a stator with 11 GRP blades, a GRP cowl of 612mm inner diameter and 12mm thickness, and a inlet bell of elliptical profile with outer diameter 762mm. This structure is supported by a steel U-stand and rotating floor stand, allowing pan and tilt. This machine produces approximately 43mph, weighs 63kg and fulfills the requirements of the brief.

Acknowledgements

I would like to acknowledge the following people and organisations for their contributions to this work:

Dr John Chick, my supervisor, for his guidance and patience throughout this project, as well as providing some interesting insights and practical knowledge.

Dr Frank Mill and Mr Chris Sturgeon for their respective expertise in Solid Edge and manufacturing and for carefully explaining concepts and methods to me.

The staff at Artem, most notably Mike Kelt, Richard North and Alex Mayes for providing the brief for the project, their insight into possible manufacturing capabilities and their tolerance in replying to my many questions.

Dr Jane Blackford for supporting me throughout my university degree.

My aunt and mum for their superior grasp on grammar and syntax, and their systematic help in correcting mine.

Summary of Resources

As this project was in collaboration with an outside company, Artem, the resources used within the University of Edinburgh were minimal. The computer laboratories in King's Buildings were used for accessing ANSYS, and the time of the staff mentioned, particularly a weekly meeting with Dr John Chick.

Word Count

Chapter	Word Count
1. Introduction	573
2. Literature Review	1,863
3. Fluid Dynamics and Fan Aerodynamics	1,836
4. Design	3,989
5. Manufacturing	294
6. Discussion	971
7. Conclusions and Further Work	427
Total	9,953

Contents

Declaration	i
Abstract	iii
Acknowledgements	v
Summary of Resources	vi
Word Count	vii
List of Figures	xi
List of Tables	xiii
List of Equations	xiv
Nomenclature	xiv
1 Introduction	1
1.1 Background and Motivation	1
1.2 Objectives	3
1.3 Structure of Report	3
2 Literature Review	4
2.1 Wind Machines	4
2.2 Fans	4
2.2.1 Aerofoil Theory	5
2.2.2 Axial-Flow Fans	6
2.2.3 Centrifugal Fans	6
2.2.4 Cross-flow Fans and Blowers	8
2.2.5 Bladeless Fans	9
2.2.6 Designing Fans	9
2.2.7 Noise	11
2.3 Summary	12
3 Fluid Dynamics and Fan Aerodynamics	14
3.1 Governing Equations	14
3.1.1 Conservation of mass and momentum	14

3.1.2	Thermodynamics	15
3.2	Fan Aerodynamics	15
3.2.1	Euler Equation of Turbomachinery	15
3.2.2	Static and Dynamic Pressure and Pressure Losses	15
3.2.3	Fan Blade Aerodynamics	19
3.3	Flow Characteristics	19
3.3.1	Boundary Layer	20
3.3.2	Separation	20
3.3.3	Recirculation	22
4	Design	24
4.1	Design Procedure Overview	24
4.2	Identify Feasible Designs	24
4.3	Impeller Design	24
4.3.1	Size	25
4.3.2	Blade Profile	27
4.3.3	Number of Blades and Chord Length	28
4.3.4	Hub-to-Tip Ratio	28
4.3.5	Materials	28
4.4	Stator	30
4.5	Motor	32
4.6	Housing Design	32
4.6.1	Inlet Bell	32
4.6.2	Safety Guards	35
4.7	Stand	36
4.8	Modelling and Optimisation	36
4.8.1	Vibrations and Vibrational Noise	38
4.8.2	Aerodynamic Noise	38
4.8.3	Modelling Aerodynamic Noise	40
5	Manufacturing	46
5.1	Assembly	46
6	Discussion	49
6.1	Evaluation of Design	49
6.2	Evaluation of Noise and Vibration Modelling	50
6.2.1	Acoustic Modelling	50
6.2.2	Modal Analysis	50
6.3	Comparison of Project to Objectives	50
7	Conclusions and Further Work	52
7.1	Conclusion	52
7.2	Further Work	52
A	Motor Power	58
A.1	Initial Euler Equation of Turbomachinery	58

B Performance Curves	59
B.1 Number of Blades PAG	59
B.2 Angle of Blades	59
C Stator	61
C.1 Flow Vectors for Stator Profile	61
C.2 Blade Dimensions	61
D Bolts	63
D.1 Stand Bolts	63
E Static Balance	66
F U-Stand Loading	68
G Project Planning	70

List of Figures

1.1 Steam punk style motorbikes for 2012 paralympic closing ceremony, produced by Artem [2].	1
1.2 Artem's current small wind machine [1].	2
2.1 Artem's larger electric wind machine.	4
2.2 Schematic of an aerofoil showing lift and drag forces, angle of attack and chord length [14].	5
2.3 Diagram of tube axial, vane axial and propeller fans adapted from [12, 70].	6
2.4 Operating curves for axial-flow fans [12].	7
2.5 Schematic of Centrifugal Fan [43].	8
2.6 Dyson air multiplier, a bladeless fan [15].	9
2.7 Schematic of forward and backward blade sweep compared to usual radial blade stacking scheme [47]	10
2.8 Schematic of static losses in fans [25].	11
3.1 Left: Rotor entry plane. Right: Velocity vectors, absolute and relative blade motion [37].	16
3.2 Aerodynamic forces acting on fan blade [37].	17
3.3 Static Pressure vs. Air Volume for a Vaneaxial Fan with Large Hub-to-Tip Ratio [12].	18
3.4 Schematic of flow over a semi-infinite flat plate, to demonstrate the formulation of boundary layer [7]	20
3.5 The inner, outer and overlap layer laws relating velocity profiles in turbulent wall flow [36]	21
3.6 Smoke Visualisation showing stalled flow on the upper surface of an aerofoil lifting vane [36]	22
4.1 Final wind machine model in Solid Edge® [58].	25
4.2 Design Process Schematic	26
4.3 Variety of blades produced by Hascon® [49]	27
4.4 Performance and efficiency curves of M type blade at motor speed 1400rpm [50]. .	29
4.5 The Moody Chart for pipe friction with smooth and rough walls [36].	30
4.6 Logarithmic wall layer chart for smooth and rough walls [36].	31
4.7 Dimensioned drawings of fan housing, created in Solid Edge® [58].	33
4.8 Air flow entering a) a round duct and b) a round duct with a venturi inlet at the duct entrance [12]	34
4.9 Schematic of an ellipse with labelled dimensions a & b.	34

4.10 Surface Shear Stress Contour Depiction of a) no inlet bell b) inlet bell with elliptical profile a=100mm and b=37.5mm and c) inlet bell with elliptical profile a=230mm and b=86mm developed using ANSYS® [60]	35
4.11 Turbulent Eddy Frequency Contour Depiction of a) no inlet bell b) inlet bell with elliptical profile a=100mm and b=37.5mm and c) inlet bell with elliptical profile a=230mm and b=86mm developed using ANSYS® [60]	35
4.12 Turbulent Kinetic Energy Contour Depiction of a) no inlet bell b) inlet bell with elliptical profile a=100mm and b=37.5mm and c) inlet bell with elliptical profile a=230mm and b=86mm developed using ANSYS® [60].	36
4.13 Fan stand, allowing rotation, from Roger George Special Effects [67].	37
4.14 Cowl modal analysis in Solid Edge® [58].	38
4.15 Stand Modal Analysis in Solid Edge	39
4.16 Directivity and streamline schematics for elementary noise sources; a) monopole b) dipole and c) quadrupole (adapted from [9]).	39
4.17 Summary of aeroacoustic source mechanisms relevant to turbomachinery noise [9].	40
4.18 Orthogonal Quality Checking of Mesh in Ansys®	42
4.19 Skewness Quality Checking of Mesh in Ansys®	43
4.20 Contour Display of Broadband Acoustic Analysis in Ansys®	44
4.21 Sound power and pressure bar chart for M blade impeller from Qualyfan [50].	45
5.1 GRP Part for bell-inlet with Artem logo relief	47
5.2 Motor keyway dimension [71]	48
B.1 Performance curves for PAG impeller with 5, 9 and 12 blades [50]	60
C.1 Mean-line Flow Schematic with Velocity Vectors	62
D.1 Schematic of Bolt Configuration for U-stand and Fan Housing Interface	65
E.1 Free Body Diagram for Static Balance of Components in Fan Housing	67
F.1 Free Body Diagram of U-Stand Loads	69
G.1 Gantt chart used for project planning compared to the actual time taken for the activities	71

List of Tables

1.1	Design Requirements for Wind Machine	2
4.1	Hascon® Blade Parameters	27
4.2	Material Properties of GRP, Aluminium and Steel, data from [66]	34
B.1	Specification of Impellers [50]	59
B.2	Specification of Impeller with Different Blade Angles [50]	59
G.1	Task Definition for Gantt Chart	70

List of Equations

3.1 Conservation of Mass	14
3.2 Conservation of Momentum	14
3.3 Navier Stokes Equation	15
3.4 First Description of Euler Equation of Turbomachinery	15
3.5 Second Description of Euler Equation of Turbomachinery	15
3.6 Third Description of Euler Equation of Turbomachinery	16
3.7 Fan Efficiency	16
3.8 Incremental Drag Force	19
3.9 Incremental Lift Force	19
3.10 Reynolds Number	19
4.1 Cascade Efficiency	28
4.2 Differential of Cascade Efficiency Equation	28
4.3 Ffowcs Williams and Hawkings equation for acoustic pressure	41

Nomenclature

Roman Letters

<i>b</i>	Acceleration
<i>c</i>	Absolute Velocity
<i>c</i>	When followed by subscript D,L or p is the coefficient of drag, lift or heat, respectively
<i>D</i>	Diameter
<i>e</i>	Exergy
<i>e</i>	Mechanical Work
<i>F</i>	Force
<i>f</i>	Frequency
<i>h</i>	Enthalpy
<i>l</i>	Chord Length
<i>M</i>	Torque
<i>m</i>	Mass
<i>Ma</i>	Mach Number
<i>n</i>	Number of...
<i>P</i>	Power
<i>p</i>	Pressure
<i>Q</i>	Volumetric Flow Rate
<i>q</i>	Heat Added to System
<i>r</i>	Radius
<i>Re</i>	Reynolds Number

<i>s</i>	Pitch - The distance between similar points in two consecutive blades
<i>T</i>	Lighthill's Stress Tensor
<i>t</i>	Time
<i>U</i>	Internal Energy
<i>u</i>	Peripheral Velocity
<i>V</i>	Volume
<i>w</i>	Relative Flow Velocity
<i>x</i>	Displacement

Greek Symbols

α	Angle of Absolute Velocity
β	Angle of Relative Velocity
Δ	Difference
δ	Change in
η	Efficiency
λ	Second Coefficient of Viscosity
μ	Coefficient of Viscosity
v	Velocity of Surface
ρ	Density
σ	Solidity
τ	Shear Stress
Φ	Flow Coefficient
Ψ	Work Coefficient
ω	Angular Velocity

Auxiliary

\cdot	Rate
$-$	Average

Superscripts

* Stagnation

Subscripts

1 Rotor Inlet

2 Rotor Outlet

3 Stator Outlet

∞ Free and Uniform

b Blades

D Drag

i A vector. i.e. for a 3D space vector will have x,y and z components

L Lift

m Mean

s Static

t Total

w Work

z Z-axis Component

α Azimuthal Component

fan Fan

hub Hub

$loss$ Negative Change in Property

pot Potential

$shaft$ Motor Shaft

Acronyms

CAD Computer Aided Design

CFD Computational Fluid Dynamics

CNC Computer Numerical Control

DNS Direct Numerical Simulation

FFT Fast Fourier Transform

FWH Ffowcs Williams and Hawkings

GRP Glass Reinforced Plastic

LES Large Eddy Simulations

LRT Lighthill Ray Tracing

PAG Glass Reinforced Polyamide

PPG Glass Reinforced Polypropylene

PU Polyurethane

RANS Reynolds Averaged Navier Stokes

SPL Sound Pressure Level

Chapter 1

Introduction

1.1 Background and Motivation

Wind machines are utilised for a range of activities in the entertainment industry to evoke atmosphere in fashion shoots, films and adverts. A number of companies, including Artem, produce these machines for such uses. Artem produces props and sets for film and TV all over the UK and wind machines are amongst their most demanded equipment. They created the wind for the national and Olympic flags, and also designed five petrol-driven wind machines that were mounted on steampunk style motorbikes for the Paralympic closing ceremony (as seen in Figure 1.1) [1].



Figure 1.1: Steam punk style motorbikes for 2012 paralympic closing ceremony, produced by Artem [2].

Artem owns three types of wind machine, larger petrol and three phase electric machines as

well as a much older and smaller, one phase machine, see Figure 1.2. The company is looking for a new small electric wind machine to be designed and built to replace this one. It should use a 240v electric motor with variable speed limit.



Figure 1.2: Artem's current small wind machine [1].

A wind machine consists of a main fan design, a motor, protective guards, mount and a stand which should be fitted to wheels for easy transportation. The design will optimise between efficiency, size, weight and cost. The main element, the fan, is a well-researched component. This project will look at advancement in wind turbine and fan technologies in order to produce a successful product. The context of films and TV adds particular considerations. The three most important factors are wind speed, air volume and noise.

Noise is very important on set and needs to be minimised. The wind speed must be sufficient to blow small objects (e.g. rain or leaves) around the set whilst the area of its influence (air volume) must be satisfactory so that multiple machines are not unnecessarily needed. Additional design requirements and preferences are tabulated in Table 1.1.

Design Requirements	Critical(C)/Preferable(P)
Minimise Costs	C&P
Ease of Manufacturing	C
Fit through a normal door	C
Tilt and Span capabilities, locked separately from wheels	C&P
Wheels Lock	C
Safe (CE Marking)	C
Method of lifting (e.g.: Fork Points)	C&P
Wind Speed 40 mph	C&P
Minimise Noise	C&P
Sufficient Air Volume	C&P
Minimise Weight (able to be lifted by two people)	C
Manoeuvrable	C
Design Cues from Artem's Larger Wind Machines	P

Table 1.1: Design Requirements for Wind Machine

1.2 Objectives

Based on the nature of the project a number of main objectives have been identified:

- 1. Understand key engineering concepts to design the structure of the wind machine.**
- 2. Perform noise analysis on various fans.**
- 3. Develop and perform an optimisation process in order to determine the optimum design.**
- 4. Develop a set of models of possible wind machines using CAD.**
- 5. Manufacture the machine.**
- 6. Assess the success of the wind machine design.**

1.3 Structure of Report

Chapter 2 of this thesis will examine the literature pertinent to this study and supporting background material. Chapter 3 covers the basic theory and fundamental principles of wind machine design. The design parameters are described in Chapter 4, followed by the manufacturing process in Chapter 5. The final design is evaluated and discussed in Chapter 6, before finally concluding the outcomes in Chapter 7.

Chapter 2

Literature Review

2.1 Wind Machines

There is limited literature on wind machines. Design cues can be taken from those currently on the market, as well as Artem's own, see Figure 2.1.

The main design feature is a fan, with customised selection criteria. Literature and advances in fan design will be comprehensively discussed in this review.



Figure 2.1: Artem's larger electric wind machine.

2.2 Fans

Turbo-machines have been extensively investigated due to their prevalent role in society dating back for centuries, including in mining, building-cooling and aeronautical applications. The first air-treating machines relating to the fan can be dated as far back as 1556; which was used for mining activities [3].

Much of fan technology advancements stem from aeronautical industries. Some of the first attempts at cohesive rotor theory was in relation to steamship navigation, resulting in a simple one-dimensional momentum theory of screw propellers by Rankine and Froude [4, 5]. Circulation and lift theories were developed by Kutta and Joukowsky [6]. Okulov et al. commended Joukowsky, Vetchinkin, Prandtl and Betz for their advancements in this field [6]. Ultimately, this produced the theoretical understanding now used to calculate rotor blades, model fan systems using the actuator disc theory and understand the vortex phenomena [7, 8].

Fans work according to the conservation of mass, momentum and energy. The working fluid (i.e. air) is compressed and moved by the dynamic rotation of the blades of the impellers, transferring mechanical energy from the fan shaft to the air in the form of increased velocity/pressure [9]. Euler and Bernoulli developed calculations used to determine the required torque that can be applied to a shaft of a rotating machine in association with these laws of conservation, allowing mathematical analysis of the specified variation of velocities through the rotor [10]. It is important to understand the mathematical principles and limitations associated with the design of fans.

2.2.1 Aerofoil Theory

The pillar of turbomachinery design is the aerofoil. Most designs of fan impellers consist of an aerofoil section, an exception being sheet metal blades whose performance are considerably lower. A typical aerofoil is seen in figure 2.2.

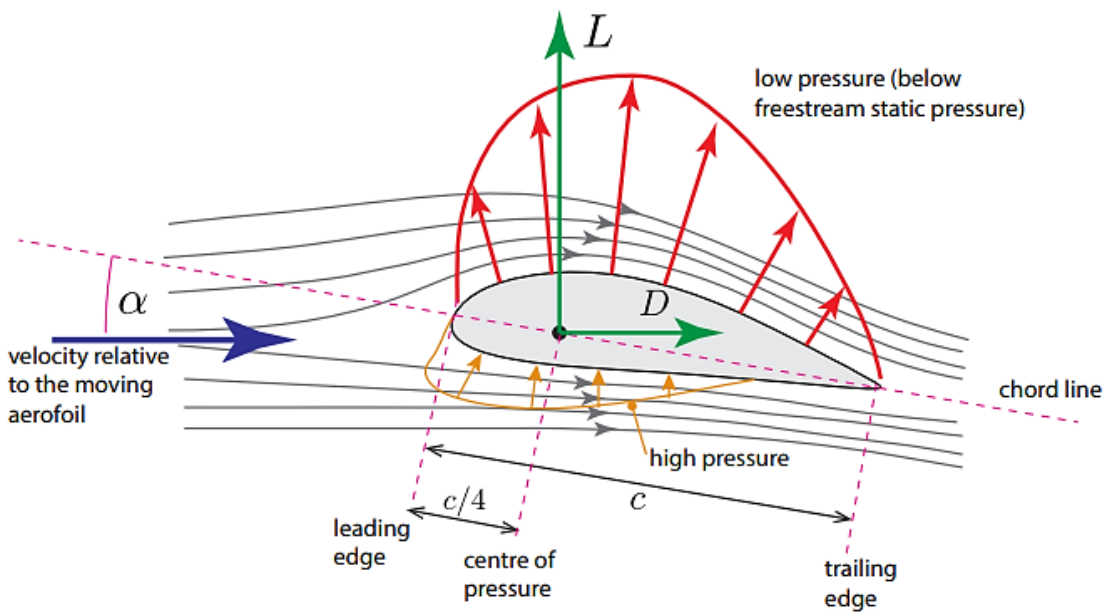


Figure 2.2: Schematic of an aerofoil showing lift and drag forces, angle of attack and chord length [14].

There is no dominant aerofoil shape, it is application dependant. For high pressure fans a high

cambered aerofoil is implemented. If efficiency is more important then a low-cambered shape is preferred [12]. These conditions will be considered in the selection of the rotor blades.

2.2.2 Axial-Flow Fans

Axial-flow fans produce air flow parallel to the axis of rotation. They are characterised by large flow rates and moderate fan pressure [9].

Axial flow fans have been well-researched for many years. In 1937 Ruden investigated theoretically and experimentally the design of a single-stage axial fan [13]. Wallis describes their increased use and advancements with duct attachments to increase efficiency and reduce noise [14]. Axial fans can be split into three categories: propeller, vane-axial and tube-axial. Selection depends on the pressure characteristics of the systems, see Figure 2.4 [12].

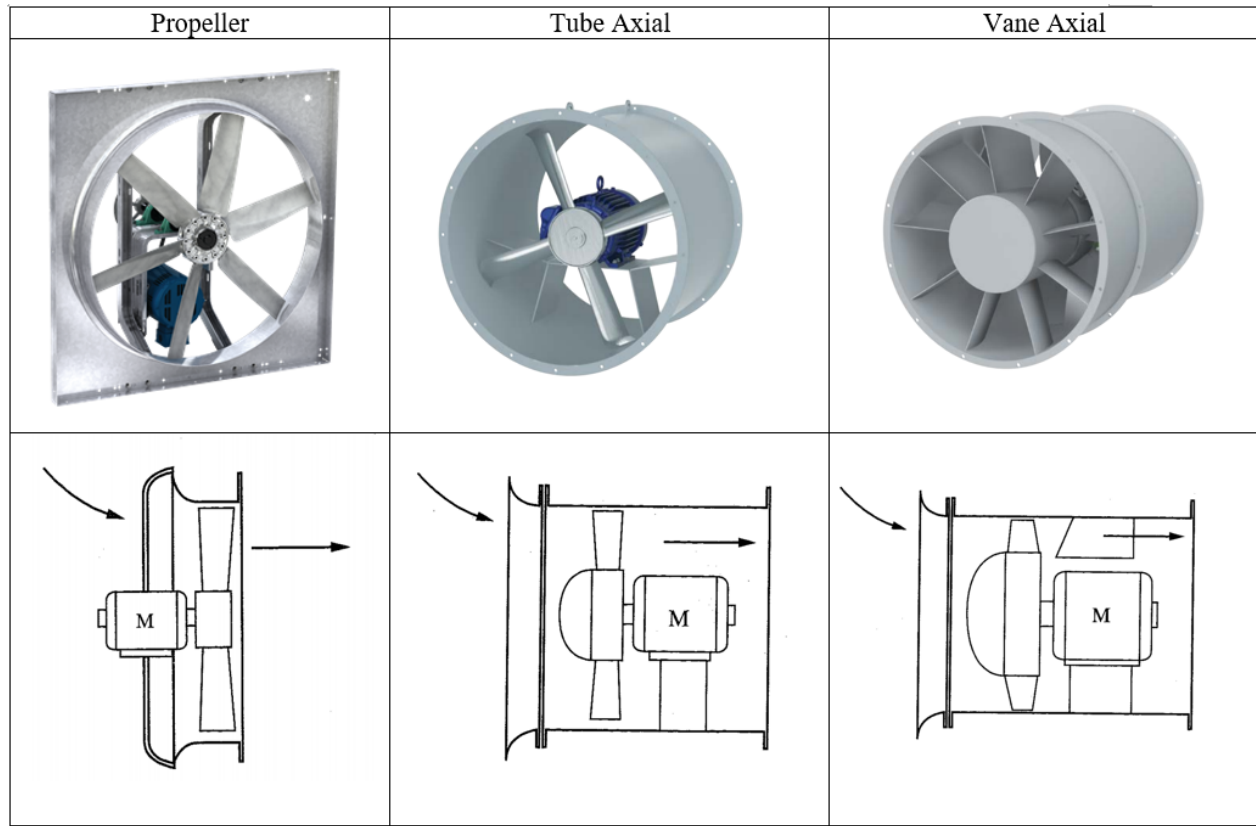


Figure 2.3: Diagram of tube axial, vane axial and propeller fans adapted from [12, 70].

2.2.3 Centrifugal Fans

Centrifugal fans expel air radially, see Figure 2.5. They normally operate in volute casings without guide outlet vanes with the casing spiral guiding the flow. The casing converts the kinetic flow energy to potential energy and increases the static pressure [11]. The best aerodynamic design is with a backward curved aerofoil blade and a curved shroud [12]. There are five other types of centrifugal fan, categorised by their blade design which impact the pressure and flow characteristics. In order

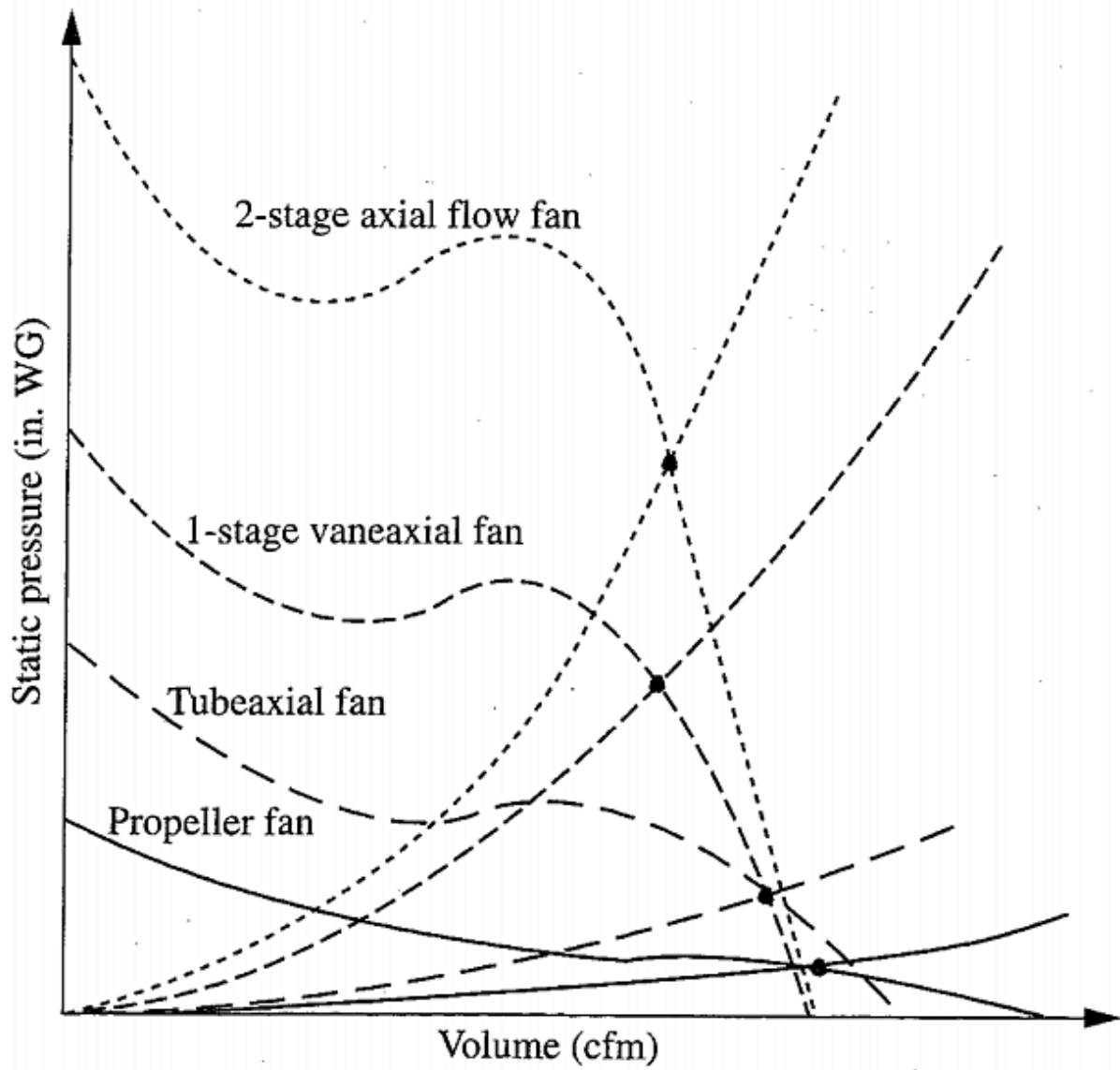


Figure 2.4: Operating curves for axial-flow fans [12].

of decreasing efficiency; Centrifugal fans with AF (Aerofoil Blades), with Backward Curved (BC), Backward Inclined (BI), Radial Tip (RT), Forward Curved (FC) and Radial Blades (RB).

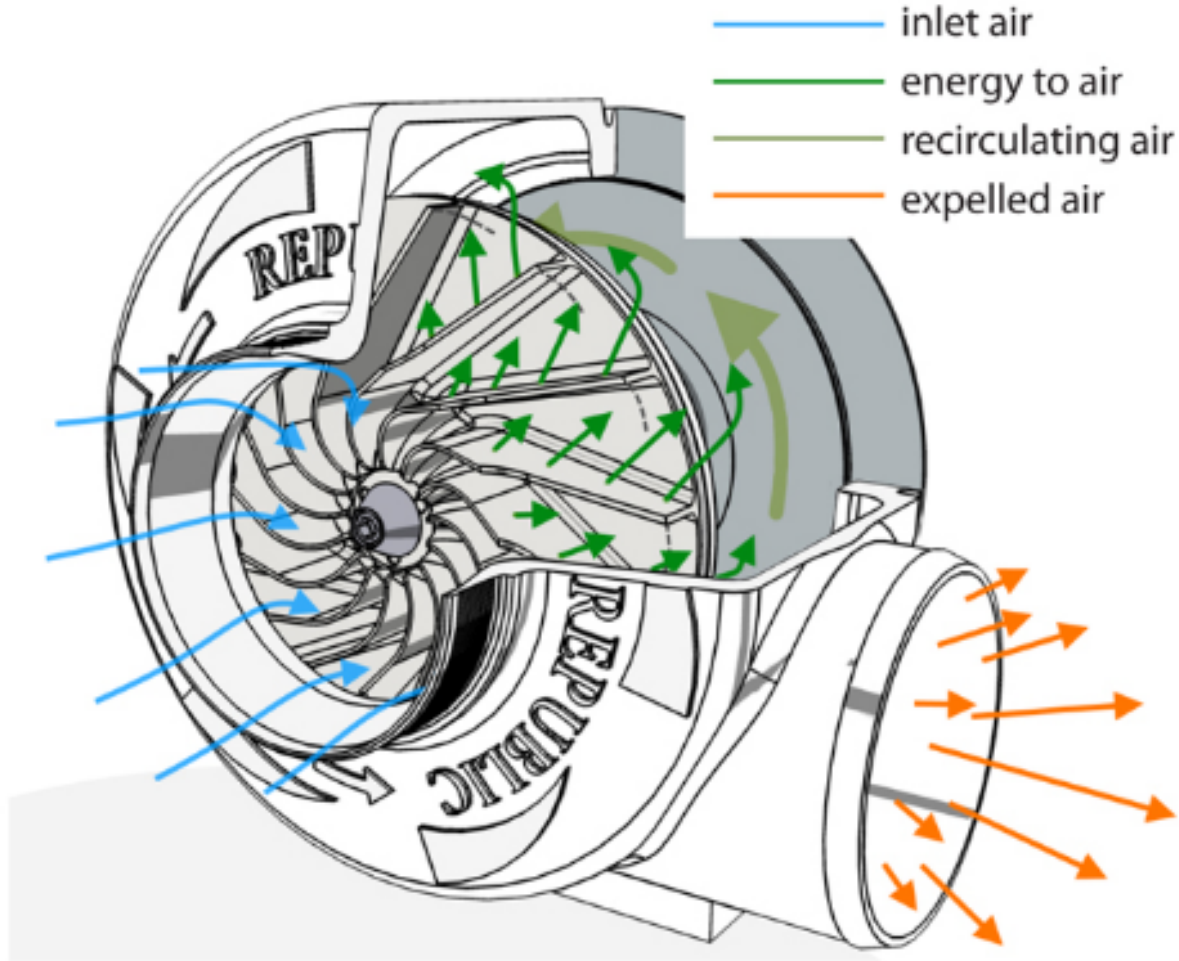


Figure 2.5: Schematic of Centrifugal Fan [43].

2.2.4 Cross-flow Fans and Blowers

Cross-flow fans are characterised by an impeller drum with forward curved blades which are usually simple circular arcs, similar to centrifugal impeller with FC blades [9]. Due to weak structural design, cross-flow fans typically run at much lower tip speeds than other fan types. However, due to their blade shapes they can handle large flow rates against relatively high back pressures.

Blowers are essentially centrifugal fans incorporating a drum impeller with a large number of forward curved blades of short radial extent. They have a similar efficiency to cross-flow fans, ranging between 30-70% [12].

2.2.5 Bladeless Fans

Bladeless fans are the latest advancement, produced by Dyson and called the Dyson Air Multiplier [15]. The distinguishing feature of this machine is the lack of external blades, see Figure 2.6.

It consists of a cylindrical base stand, in which the electric motor and internal blades draw air in. This base supports a hollow aerofoil shape ring with a 1.3 mm narrow slit which acts as a jet nozzle and produces airflow at approximately 24 m/s [15, 16].

The major advantage of the bladeless fan is the reduction in noise due to its far-field laminar flow, for which Dyson received an award from the Noise Abatement Society [17]. As none of the blades are exposed for fingers or debris to be trapped, it is safer. Unfortunately the technology is new and the parts bespoke, Dyson have applied strict patenting licenses to stop ‘knock-off’ designs being created which means that this is not a viable design for this project [18]. In the future this may be a good solution for wind machines provided sufficient wind speeds are achieved.

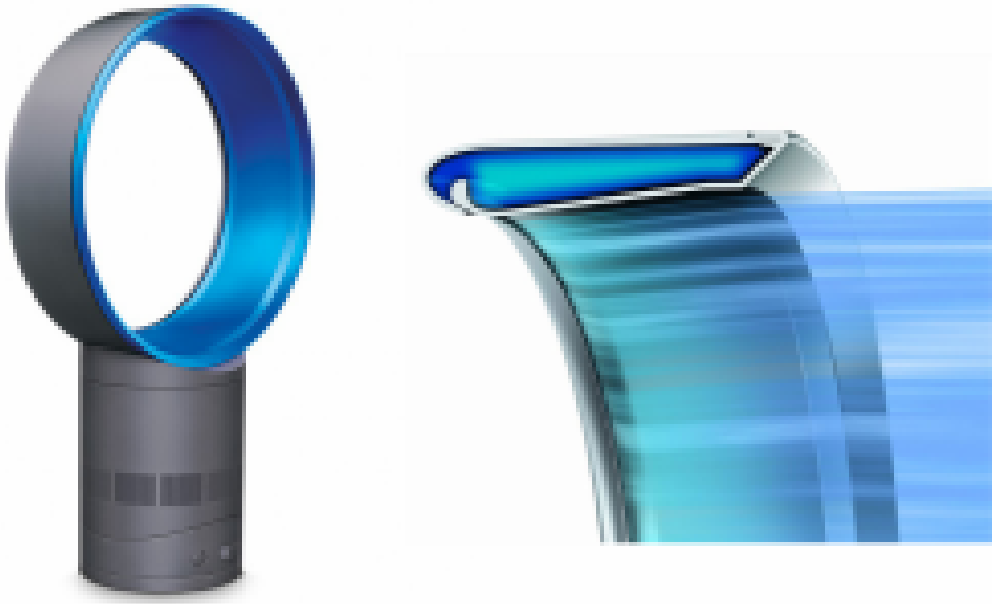


Figure 2.6: Dyson air multiplier, a bladeless fan [15].

2.2.6 Designing Fans

Van Niekerk minimised empirical methods and assumptions used in the design procedure. He attempted to reduce noise and included this as a design parameter [19]. Bass distinguished between two different fan design routines, an isolated aerofoil approach and a rotating cascade approach [20]. Smith promoted the use of a simple three dimensional approach to an axial flow fan [21].

These developments have determined the current process in fan design: blade design (chord, twist etc.), hub-tip ratio, tip clearances and operating range. These decisions will specify the efficiency, flow and noise characteristic of the fan and must adhere to design requirements.

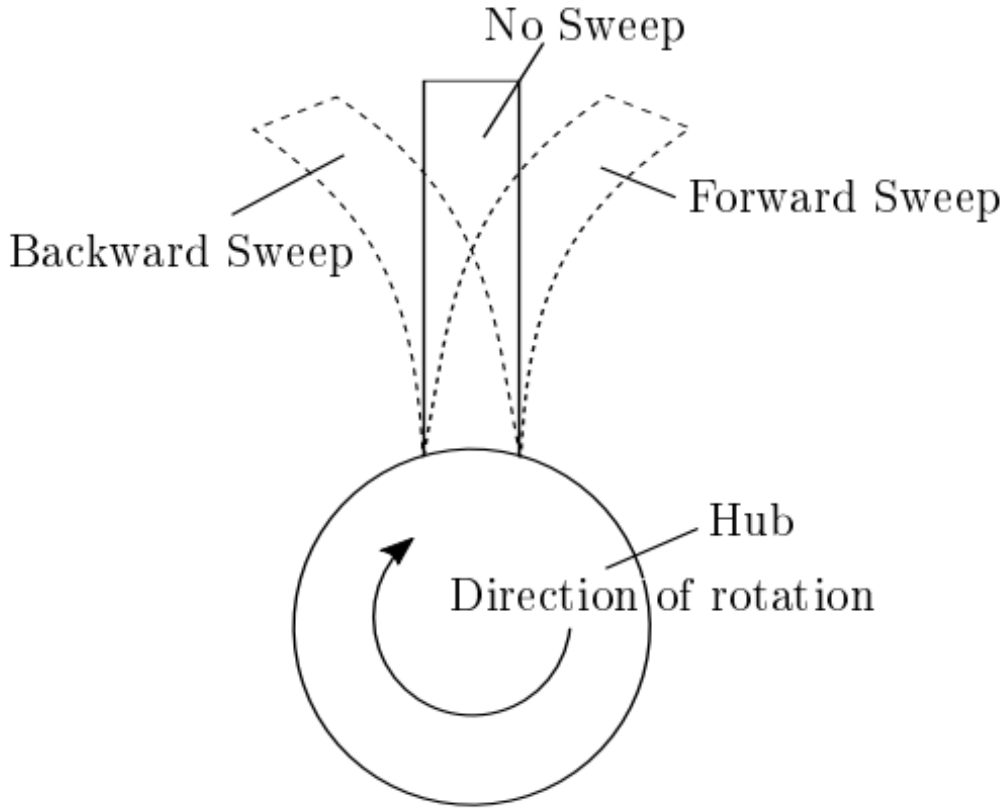


Figure 2.7: Schematic of forward and backward blade sweep compared to usual radial blade stacking scheme [47]

Blade Design

For good efficiency, the airflow should be distributed evenly over the working face of the fan. The axial air velocity should be the same from hub to tip which can be achieved through blade twist, with larger angles near the centre.

The static pressure should be even over the blade. Due to lower relative velocity at the hub this should be countered with larger lift coefficient and chord length. The chord length is limited by blade overlap and the lift coefficient has a fundamental maximum [12]. The blades must not overlap at the hub, as this may choke the airflow.

The number of blades is another design criteria. This design process will have to balance the number of blades according to noise, efficiency and weight.

Blades with sweep, see Figure 2.7, are known to have benefits such as drag reduction at higher Mach numbers [47]. Beiler and Carolus found that back sweep tends to negatively impact fan performance with flow separation occurring at relatively high flow rates [59]. Forward sweep can result in better outlet flow distribution, reduced discharge losses and noise emissions, and improved acoustic performance.

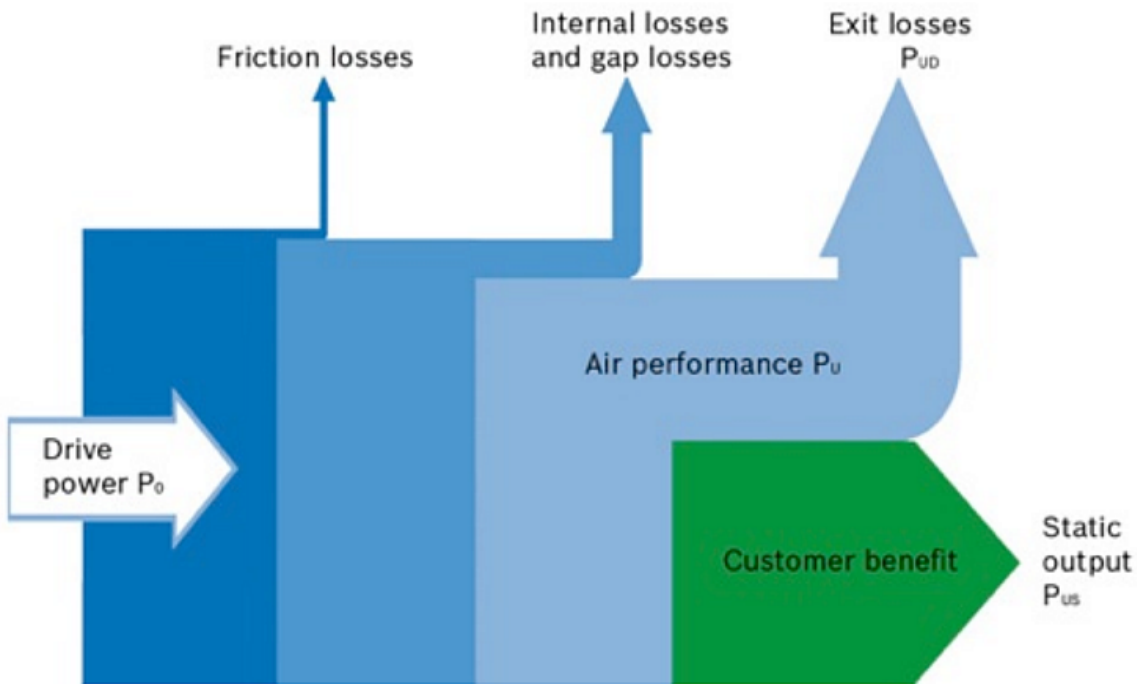


Figure 2.8: Schematic of static losses in fans [25].

Hub-to-Tip Ratio

The hub diameter is determined by a function of static pressure and speed, meaning that it can be selected from the system requirements. The wheel diameter is a function of hub diameter and cfm/rpm.

Operating Range

Fans are characterised by a stalling range; this is when they become very noisy and inefficient. To avoid this the maximum operating pressure of the selected unit should be 30-50% higher than the pressure required for the application [12].

2.2.7 Noise

Noise is a major optimisation parameter for wind machines. It is largely due to complex flow fields involved in and around the impeller which are still not well understood [22]. It is important due to its association with losses (and consequent lower fan efficiency).

Many noise mechanisms may occur, not all of which relate to poor performance. Some noise generators are fundamental to the function of a fan (e.g. vortex shedding). High levels of noise can be associated with lower efficiency fans, indicating power losses, see Figure 2.8.

Noise Classification

The first propeller noise studies appeared in the 1930s [23, 24], and were largely led by the aeronautical industry. For this reason, axial turbomachinery have been given greater attention than centrifugal fans [9].

Noise can be associated with aerodynamic, gear, bearing, vibrational and drive motor noise, aerodynamic being the most dominant [9]. Wright and Cumpsty pioneered the link between aerodynamic features of the fan rotor and its acoustic emissions [22, 24]. It has two major components; tonal and broadband [25], due to the steady and unsteady forces that are exerted by the turbulent flow on the blades, vanes and fan casing.

The main mechanism for noise generation are the rotor blades which generate noise as a result of turbulent wake shedding from the interaction between the end-wall boundary layer and the rotor tip [22]. This may be generated by; turbulent inflow, self-noise (boundary layer, and boundary layer separation, trailing edge noise, secondary flows), and tip leakage related noise [26].

Tip leakage flow is recognised as the major source of noise, investigated by Marcinowski [22], Inoue and Kuroumaru [27], Storer and Cumpsty [28], and Lakshminaravanan [29]. The 3D and unsteady nature of these flows influence aerodynamic losses and noise generation. Longhouse, Fukano et al. and Kameier & Neise argued that it can be one of the most significant sources correlated to the broadband spectral signatures as well as narrowband tones at frequencies below the blade passing frequency. Akaike demonstrated that the vertical structure near the rotor tip in industrial fans is one of the major noise generating mechanisms for low speed turbomachines [30].

The importance of the review of this research lies in understanding the effects of certain design cues on the systems acoustics, the tip clearance will have a significant impact on the noise characteristics of a fan according to Marcinowski [22], Mudridge & Morfey [31], Longhouse [32], Fukano & Jang [33] and Kameier and Neise [34]. Special attention should be made in designing these parameters.

2.3 Summary

The literature review has aided in addressing the objectives of the project. From this research, axial flow fans were decided to be the most appropriate due to their characteristics of producing high air flows against moderate pressure, this is discussed further in Chapter 4. The most influential parameters for the fan component have been identified as:

- Blade design, including chord length, camber, number of blades and coefficient of lift.
- Hub-to-tip ratio, which should be minimised to increase air flow but without risking stall.
- Tip clearance between the blades and the fan housing.
- Operating range, which is depicted on fan performance curves of deliverable air flow against static pressure.

The noise mechanisms of a fan have also been recognised, categorised as tonal and broadband noise sources. This allows insight into modelling aims and methods as differing noise sources should be modelled accordingly. This assists in assessing the success of the design by comparing

the most important design decisions to gauge whether they have been optimised individually and collectively.

Chapter 3

Fluid Dynamics and Fan Aerodynamics

There are a number of fluid dynamic and fan aerodynamic theories and governing equations of which a fundamental understanding is imperative for the successful design of an efficiently operating fan. Concepts including aerofoil lift and boundary layers have been introduced in the literature review. This chapter aims to provide comprehensive insight into the engineering and mathematical descriptions and reasoning behind these phenomena, including the fan performance parameters, boundary layer flow, and vortex shedding.

No general analysis of fluid motion exists yet. There are several particular solutions, many approximate digital computer solutions and a plethora of experimental data [36]. The equations outlined are subject to many assumptions and limitations for useful analytical investigation of the system. This is a simplified summary of the most relevant concepts.

3.1 Governing Equations

3.1.1 Conservation of mass and momentum

The rotating impeller of the fan transfers mechanical energy from the fan shaft to the working fluid in the form of increased velocity and/or pressure [9]. The fundamental principles of fans are conservation of mass (eq.3.1) and momentum (eq. 3.2) [36].

$$\frac{\partial \rho}{\partial t} + \frac{\partial \rho u_j}{\partial x_j} = 0 \quad (3.1)$$

Where ρ is the density, u is the velocity at a location x in time, t .

The momentum equation is derived from Newton's second law of motion. The change of momentum of a volume of fluid must be equal to the sum of the forces acting on the volume;

$$\rho \frac{D u_i}{D t} = \rho b_i - \frac{\partial p}{\partial x} + \frac{\partial \tau_{ji}}{\partial x_j} \quad (3.2)$$

This equation describes that a change in momentum density, ρu_i may be caused by the gradient static pressure in that direction $\frac{\partial p}{\partial x}$, viscous forces $\frac{\partial \tau_{ji}}{\partial x}$, and volumetric body forces ρb_i .

Eq.3.2 can be simplified for isotropic Newtonian fluids (e.g. air) by relating the viscous stress τ to the velocity gradient by a factor of dynamic viscosity μ , resulting in the Navier-Stokes Equation;

$$\rho \frac{Du_i}{Dt} = \rho b_i - \frac{\partial p}{\partial x_i} + \mu \frac{\partial^2 u_i}{\partial x_j \partial x_j} + (\mu + \lambda) \frac{\partial}{\partial x_i} \left(\frac{\partial u_j}{\partial x_j} \right) \quad (3.3)$$

where λ is the second coefficient of viscosity, defined as $\lambda = -\frac{2}{3}\mu$.

The corresponding equations are often too difficult to analyse for arbitrary flows. Researchers have focused on techniques and simplifications to achieve solutions. Prandtl discovered low viscosity fluid flows (i.e. air) can be divided into a thin viscous layer, near solid surfaces called the boundary layer, and a nearly inviscid layer, characterised by Euler and Bernoulli equations. This is one of the most important fluid dynamic principles, to be described further in this chapter.

3.1.2 Thermodynamics

In the case of a compressible flow field, further conditions need to be defined, requiring a system of equations derived from the conservation of thermodynamic energy and the equations of state. The first law of thermodynamics states that the change in internal energy of a system is equal to the sum of the heat input or output and the work done by or on the system.

3.2 Fan Aerodynamics

3.2.1 Euler Equation of Turbomachinery

The Euler equation of turbomachinery stipulates that the fan power input P_w is the product of external torque M_{shaft} and angular speed ω of the fan shaft [37];

$$P_w = M_{shaft} 2\pi f_0 = M_{shaft} \omega \quad (3.4)$$

Considering the control volume around the blade, see Figure 3.1, the force exerted on the fluid is given by the rate of change of momentum of the fluid. Given this, an alternative form of the Euler Turbomachinery Equation is:

$$P = F_\theta r_m \omega = r_m \omega \dot{m} (w_{\theta 2} - w_{\theta 1}) \quad (3.5)$$

3.2.2 Static and Dynamic Pressure and Pressure Losses

The transmission of mechanical work, e_w from the shaft to the fluid increases the local stagnation enthalpy h^* by e_w , but not all enthalpy increase from technical work is transformed into exergy, e (available energy). The sum of exergy is lower than the introduction of mechanical work e_w by the magnitude of increase in internal energy U . I.e.:

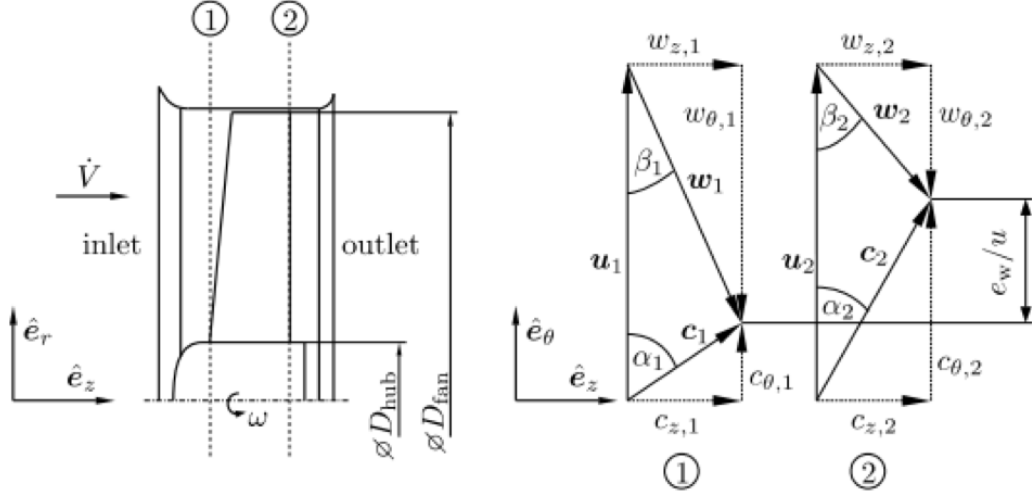


Figure 3.1: Left: Rotor entry plane. Right: Velocity vectors, absolute and relative blade motion [37].

$$\begin{aligned}
 e_w &= h_2^* - h_1^* - q \\
 &= \frac{p_{t,2} - p_{t,1}}{\rho} + u_2^* - u_1^* - q \\
 &= \frac{\delta p_s}{\rho} + \frac{1}{2}(c_2^2 - c_1^2) + \frac{\delta p_{loss}}{\rho}.
 \end{aligned} \tag{3.6}$$

This introduces the total fan pressure difference $p_t(r)$, the static pressure difference $p_s(r)$, the pressure losses, and the total fan efficiency. The same identity can be derived by applying Bernoulli's equation in a rotating system. The total fan efficiency is defined as;

$$\eta_{total} = \frac{Q\delta p_t}{P} \tag{3.7}$$

where Q is the volumetric flow rate $[\frac{m^3}{s}]$ and P is the Power supplied to the shaft.

Pressure difference is vital to the characterisation of a fan. It is used in determining the efficiency and performance curve of the fan. Axial flow fan performance curves are characterised by the shape shown in Figure 3.3.

When the fan is operating in free-delivery (i.e.: $P_s = 0$) there is peak air volume. The static pressure increases while the air volume decreases due to increasing restrictions and lift coefficient of the blade. When the maximum lift coefficient is reached, the angle of attack becomes large enough that the flow is no longer blade congruent, and separation occurs. The fan stalls, and becomes noisy and inefficient. It is critical to avoid the stalling range, hence performance curves are important.

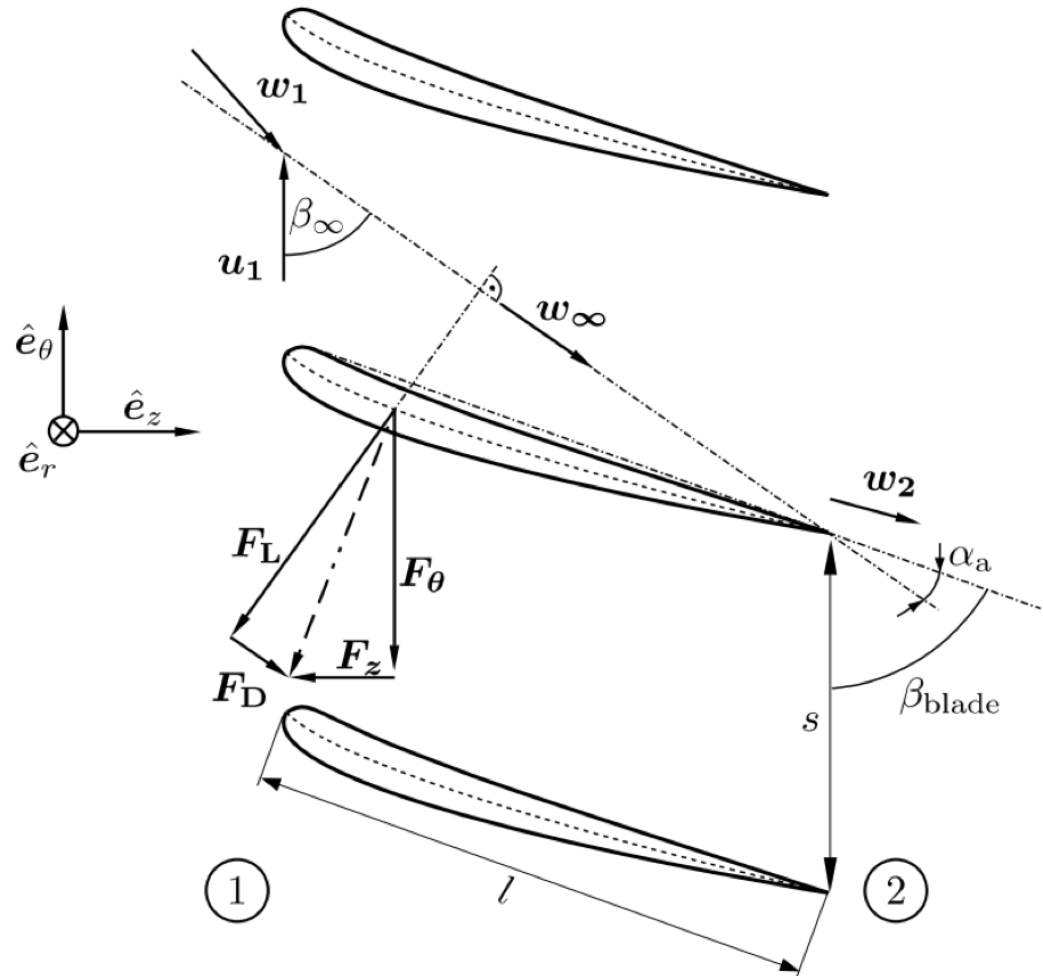


Figure 3.2: Aerodynamic forces acting on fan blade [37].

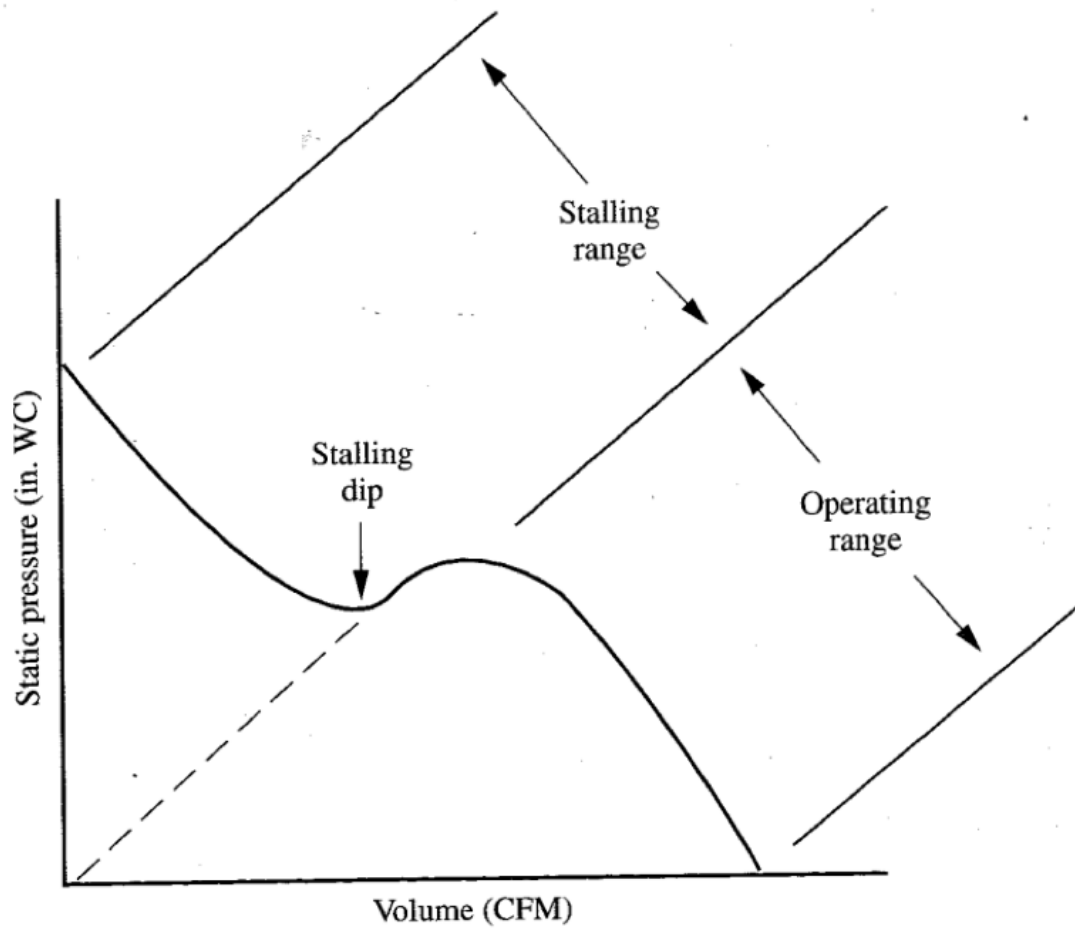


Figure 3.3: Static Pressure vs. Air Volume for a Vaneaxial Fan with Large Hub-to-Tip Ratio [12].

3.2.3 Fan Blade Aerodynamics

The change in momentum of the fluid caused by fluid-blade interaction drives the fan, and the geometry of the blade has an impact on fan performance.

The mechanism can be illustrated using a 2D aerofoil model, Figure 3.2. Inside a uniform flow field of w_∞ , any solid body decelerates the flow and experiences a drag force, F_D in the flow direction. Incremental drag force at location r in the mean relative flow w_∞ is then;

$$dF_d = c_D \frac{\rho}{2} l w_\infty^2 dr \quad (3.8)$$

where l is the chord length.

Perpendicular to F_D is the lifting force F_L , given by;

$$dF_L = c_L \frac{\rho}{2} l w_\infty^2 dr \quad (3.9)$$

Chord length, l , number of blades and hub-to-tip ratio are important for the performance of the fan, influencing the volume rate through the turbine, the stall conditions and the tip leakage.

The force of the blades on the fluid causes a change in velocity in the radial and azimuthal direction, see Figure 3.1. The relative velocities are given by w_1 and w_2 at the fan inlet and outlet, respectively. The whirl velocities are denoted by c_θ . These velocity triangles can be used to calculate the inlet and exit angles, the relative and the whirl velocities [56].

3.3 Flow Characteristics

There are a number of flow phenomena associated with turbomachinery affecting the noise and efficiency of the machine, and modelling techniques used for noise prediction. The most important of these are: boundary layer flow, recirculation and separation.

Two key parameters in fluid mechanics are Reynolds number, Re and Mach number, Ma . Re is given by,

$$Re = \frac{VL}{\nu} \quad (3.10)$$

where ν is dynamic viscosity.

This is convenient for predicting whether the flow is laminar or turbulent which determines the modelling of the system. Roughness will also have an effect on the transition to turbulent flow.

The Mach number is the ratio of the speed of a body to the speed of sound in the surrounding medium. It is important for the compressibility or incompressibility class of a system. Generally, for Mach numbers (Ma) of less than 0.3 incompressibility can be assumed [36].

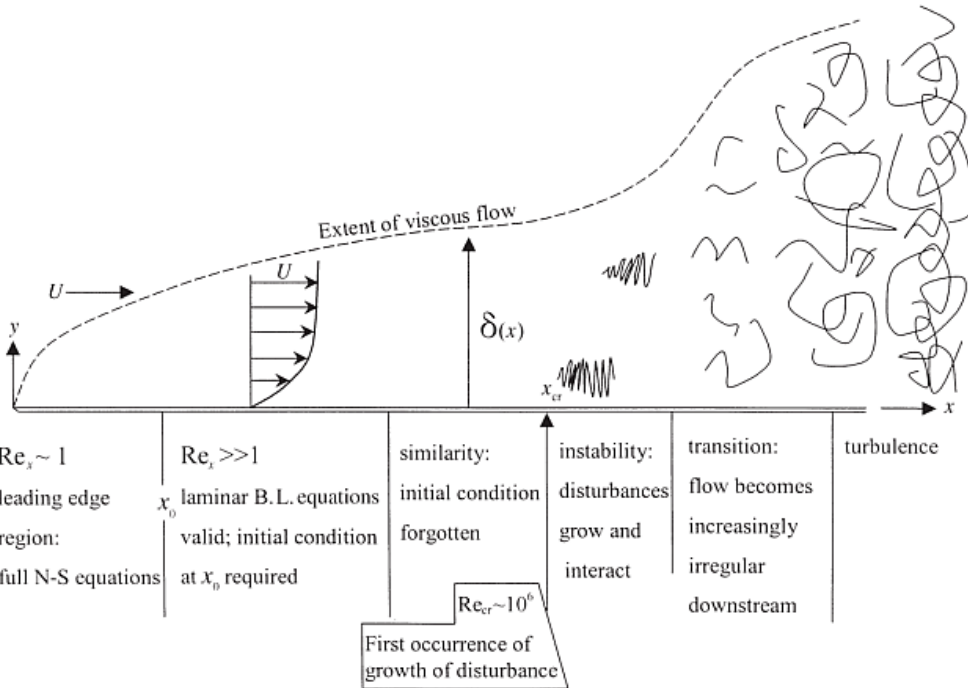


Figure 3.4: Schematic of flow over a semi-infinite flat plate, to demonstrate the formulation of boundary layer [7]

3.3.1 Boundary Layer

When the flow is contained, for example in a pipe, the friction at the wall and viscous effects through the fluid means that the effect of the walls will permeate the entire internal flow [54].

This is characterised by an entrance region, where nearly inviscid upstream flow converges and enters the tube. Viscous boundary layers then grow downstream, retarding the axial flow at the wall and accelerating the core flow, see Figure 3.4 [7].

Prandtl contributed to the generalisation of boundary layer theory. The fundamental assumption is that the layer is thin compared to other length scales. Across this layer, the velocity varies rapidly enough for viscous effects to be important [54]. There are three distinct areas, the inner wall layer dominated by laminar shear forces, the outer layer where turbulent shear layers dominate and an intermediate area, the overlap layer, where both are important. These are depicted in Figure 3.5. Typically the inner wall layer extends over less than 2% of the profile and can be neglected.

Boundary layer description is vital for turbomachinery, used to compute viscous effects near solid walls which are then ‘patched’ onto the outer inviscid motion. Viscous effects are prevalent in a fan; along the internal wall of the housing, on the blades and in the form of wakes, jets and shear layers.

3.3.2 Separation

As boundary layer thickness increases over a solid object, e.g. a rotor blade, there is excessive momentum loss near the wall due to an adverse pressure gradient. The boundary layer separates

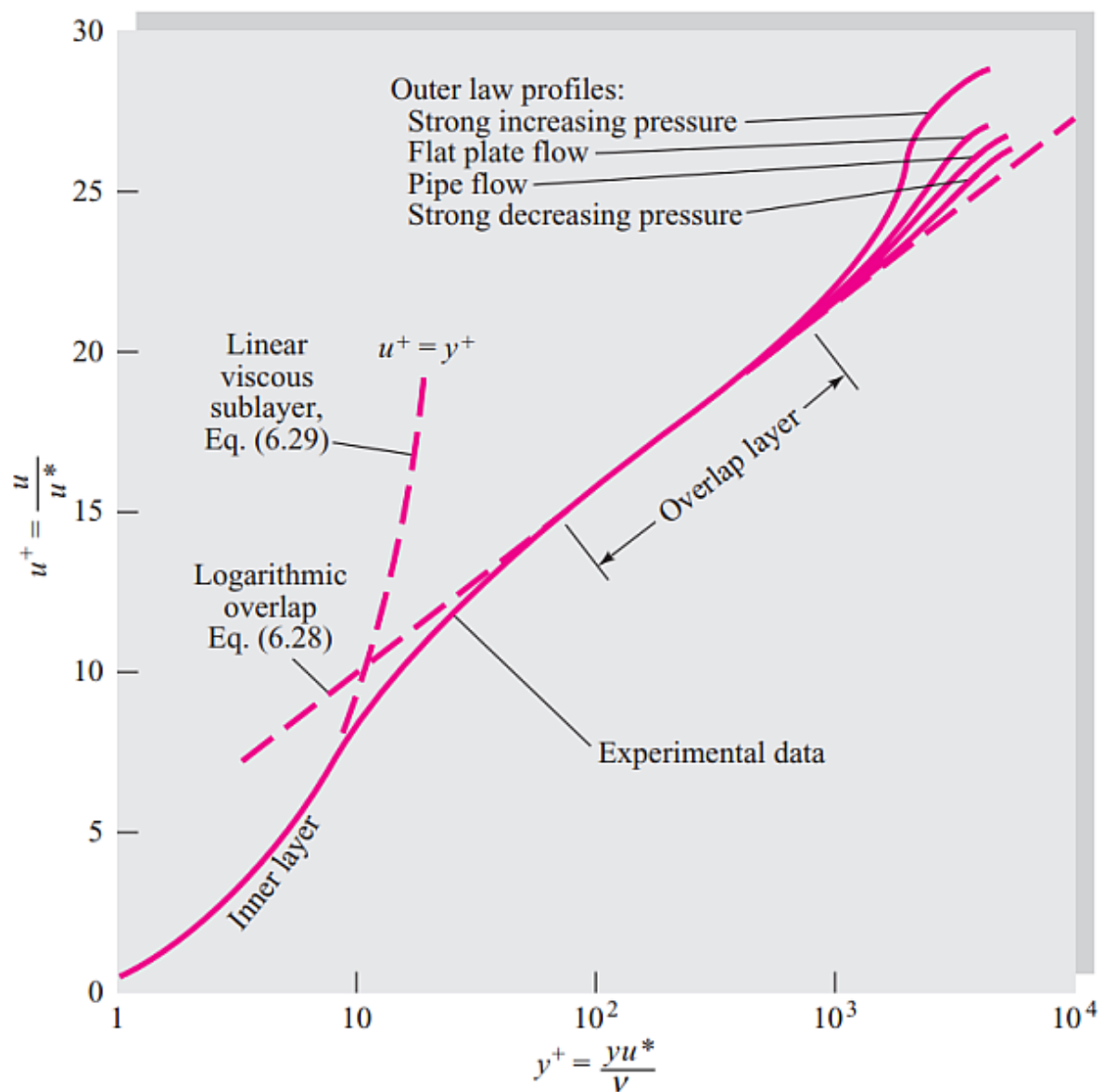


Figure 3.5: The inner, outer and overlap layer laws relating velocity profiles in turbulent wall flow [36]

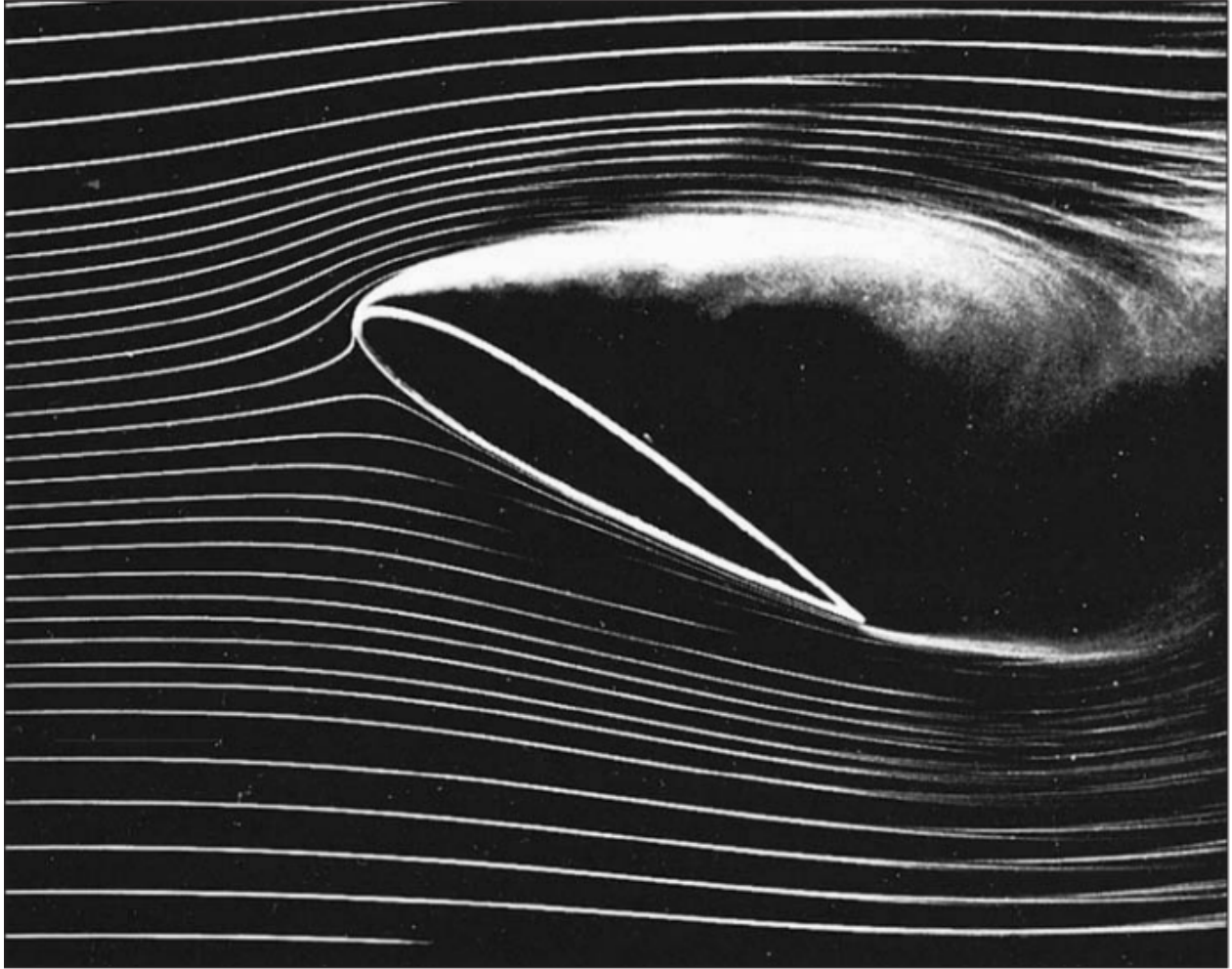


Figure 3.6: Smoke Visualisation showing stalled flow on the upper surface of an aerofoil lifting vane [36]

from the object's surface and a vortex-filled wake is formed. This increases drag and decreases efficiency, explaining the need to streamline the rotor blades.

This phenomenon explains stalling. At a low angle of attack the rear surface of an aerofoil has an adverse pressure gradient, but not enough to cause significant boundary layer separation. As the angle of attack increases, the adverse gradient becomes stronger and a separation bubble begins to creep forward. At a certain angle the flow is separated completely and the aerofoil is stalled, see Figure 3.6.

3.3.3 Recirculation

Rotor-stator interactions are main causes of recirculation, vortex formation and consequently losses and noise. When an axial fan blade turns, a pressure gradient is created from the streamline curvature described in the lift force generation. The velocity near the wall will be smaller due to viscosity and no-slip boundary at the wall. The overturning of the fan moves slow velocity fluid close to the wall from the blade pressure surface to the blade suction surface, and the motion is compensated

by a return flow near the centre of the passage. The combined effect is two three-dimensional passage vortexes in the streamwise directions [54]. These inertia-generated vortexes are also known as circulatory flow, which cause efficiency losses in the machine.

Chapter 4

Design

The design requirements are outlined in Chapter 1, Figure 1.1. The important features include the volume flow rate of air, pan and tilt and the minimisation of noise and cost.

The design was informed through research and analysis outlined in Chapters 2&3. Implications of design parameters and those vital to successful operation of the machine were assessed. Equations developed were utilised to numerically identify design options, subject to compromise and optimisation. The design was modelled on Solid Edge®, shown in Figure 4.1.

4.1 Design Procedure Overview

A step-wise design approach is presented in Figure 4.2. It is intended to be rational, robust and capable of designing an efficient wind machine.

4.2 Identify Feasible Designs

Each of these fan types were considered as a possible solution: axial, centrifugal, cross-flow, blowers and bladeless. Some of the designs (i.e. bladeless fans) were unfeasible due to patents. Centrifugal fans characteristically produce higher pressure and lower flow rate airflow than axial fans, not ideal for a wind machine. Cross-flow fans and blowers produce higher static pressure and air volume than a vaneaxial fan of the same wheel diameter. They have inferior efficiencies, and require more power.

Centrifugal and cross-flow fans are prone to higher noise levels compared to axial fans. The drastic directional change of the airflow requires obstructions and increases noise-inducing flow such as boundary layer and recirculation. As noise is important, axial fans were ultimately decided to be the most appropriate.

The axial fan consists of a rotor, stator, duct, stand, motor, inlet bell and finger guards.

4.3 Impeller Design

The impeller, or rotor, is vital to the performance of the machine. There are five main parameters to consider:

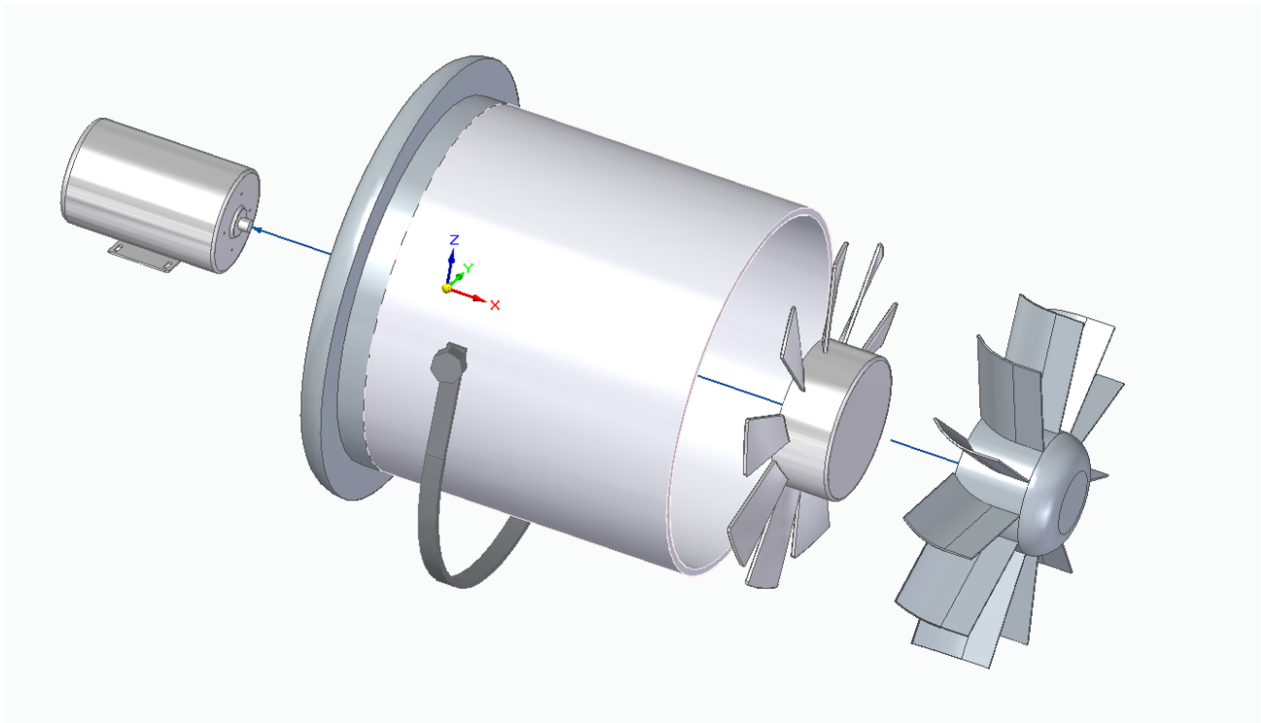


Figure 4.1: Final wind machine model in Solid Edge® [58].

1. Size
2. Blade Profile
3. Number of Blades
4. Hub-to-tip Ratio
5. Materials

The impeller must operate well within the entire range of shaft speeds of the variable speed motor (up to 1400rpm).

4.3.1 Size

The size was constrained by the dimensions of a standard door. Internal doors average between 750-800mm width, external doors are approximately 900mm [46]. The impeller size should be maximised within this constraint for greater air volume. The machine will consist of a duct, inlet bell and fixtures, which must fit within this width.

The widest structure is the inlet bell. Initial research suggested that the radius of this should be at least 14% of the housing inside diameter, in order to adequately improve the inlet flow [12].

Initial estimation defined the impeller diameter between 500-600mm. Utilising eq.3.4, initial calculations predicted wind speeds of 40-50mph (see Appendix A). The 600mm impeller was deemed acceptable in size, produced the best airflow increase, and was chosen.

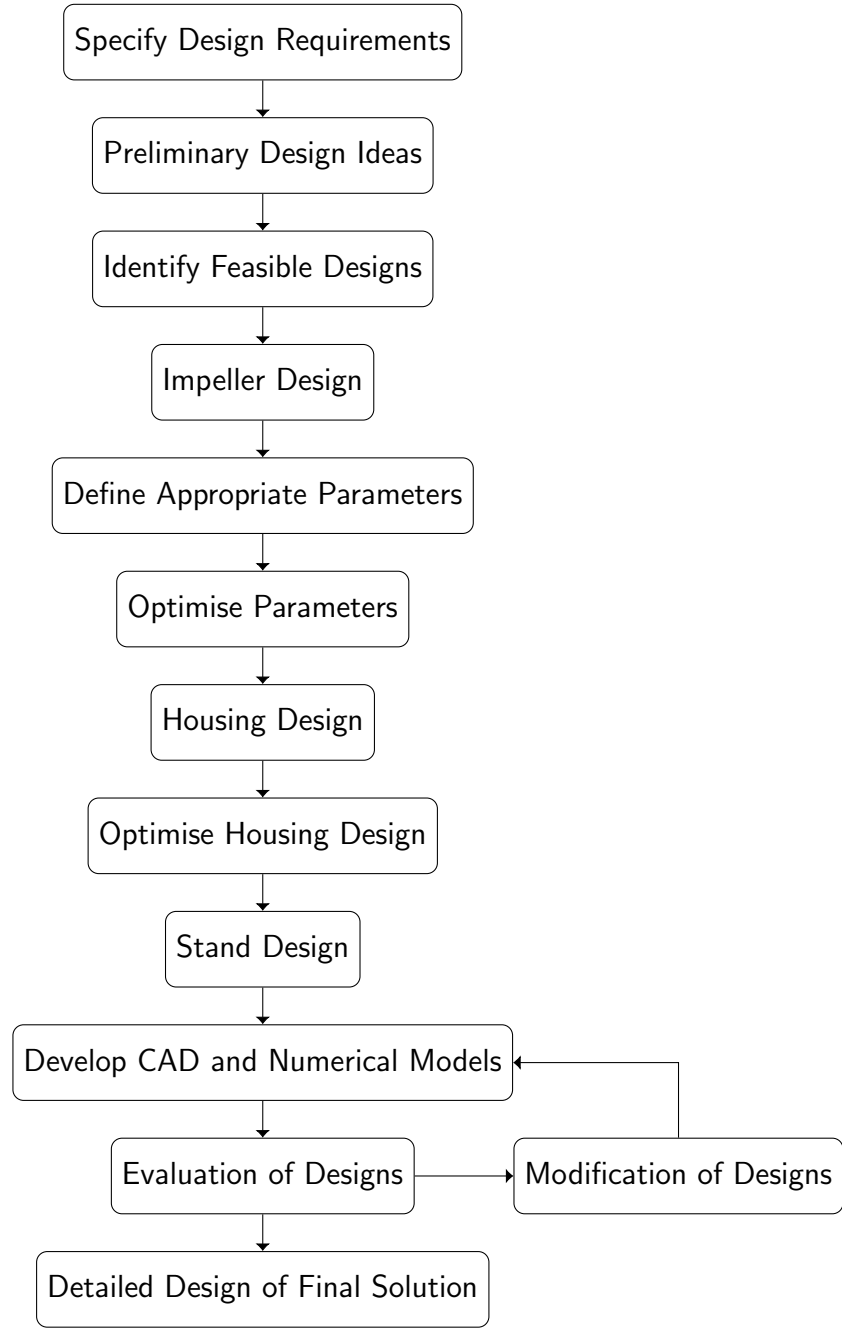


Figure 4.2: Design Process Schematic

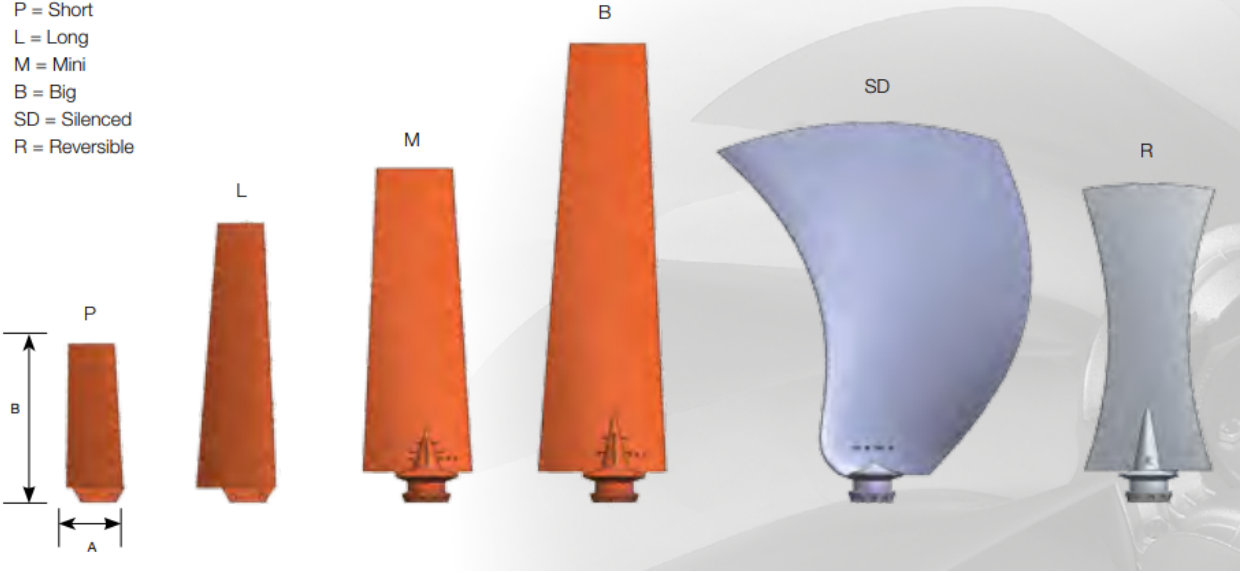


Figure 4.3: Variety of blades produced by Hascon® [49]

4.3.2 Blade Profile

Although an aerofoil profile is not critical, cheaper sheet metal is inferior for aerodynamic performance, resulting in diminished blade congruence, pronounced boundary layer flow and separation [12]. The operating range of the fan is narrower, and the fan less efficient and more noisy. Aerofoil blades are therefore justified.

The shape of the aerofoil largely determines the losses associated with the rotor, as well as the drag and lift coefficients. The selection decision is based on these coefficients, the angle of attack and the chord lengths.

The blades will be purchased from Hascon®. These impellers allow design flexibility. The hubs can be fitted with the desired number of blades set to an angle of the designer's choice. There are a variety of blades with varying geometries, chord lengths, and hub sizes, see Figure 4.3 and Table 4.1.

Blade Type	Chord length (mm)	Blade length (mm)
P - Short	65	150
L - Long	83	280
M - Mini	115	320
B - Big	135	450
SD - Silenced	120	360

Table 4.1: Hascon® Blade Parameters

After considering the performance curves, the M blade was chosen. This provides a wind speed of 43mph when the motor is running at 1400 rpm. The blades will be trimmed to 200mm long.

The 'silenced' blades are more efficient, but cost constraints mean the noise of the machine will be minimised through other design criteria. There is potential for improvements on the design here.

For angle of attack optimisation, the efficiency of a compressor blade is defined by eq. 4.1 [48];

$$\eta_D = 1 - \frac{2C_D}{C_L \sin^2 2\alpha_m} \quad (4.1)$$

where α_m is the average velocity angle across the rotor. Assuming a constant lift-drag ratio, eq. 4.1 can be differentiated with respect to α_m to give the optimum mean flow angle for maximum efficiency [48]. Thus,

$$\frac{\partial \eta_D}{\partial \alpha_m} = \frac{4C_D \cos 2\alpha_m}{C_L \sin^2 2\alpha_m} = 0 \quad (4.2)$$

so that $\alpha_{m,opt} = 45^\circ$

As the impeller will run at varying rotational speed, the selected angle must perform well over this range. The performance curves were inspected, and a pitch angle of 45° was deemed optimum, see Figure 4.4. The fan will be operating far outside of the stalling range. The chosen impeller is acceptable for the static pressure, airflow volume, and power of the motor. For the performance curves of inspected impellers refer to Appendix B.

4.3.3 Number of Blades and Chord Length

According to equations 3.8 and 3.9, the overall force on the flow from the blades is proportional to the number of blades and chord length. Flow characteristics such as turbulence, separation and vortex formation are mainly produced by the leading and trailing edges of the blades. Fewer and wider blades result in better fan efficiency and lower noise level [48]. Choking risks mean large blades require a larger hub, increasing weight and cost of the part. Compromise consisting of a fan with five to twelve blades is a good solution [12].

This impeller will utilise M type blades. They have the largest reasonable chord length. The impeller has nine blades in order to satisfy the required air flow.

4.3.4 Hub-to-Tip Ratio

The hub diameter must be large enough to prevent stalling. It also restricts air flow and should be minimised within this constraint. The hub-to-tip ratio is expected to be between 50-80% [12]. The hub diameter for this machine will be 300mm which gives a hub-to-tip ratio of 50%.

4.3.5 Materials

The material must have a sufficient strength-to-weight ratio to withstand the static, dynamic and pressure loads which it will be exposed to while minimising weight, and have a low roughness coefficient.

Turbulent flow is strongly affected by roughness. Minimal roughness heights can break up the flow's linear viscous sublayer and profoundly change the wall law, see Figure 4.6. This affects the friction, characterised by the Moody Chart, see Figure 4.5. The roughness exacerbates unsteady and turbulent flow, causing earlier onset separation and larger wake flows, reducing the efficiency of the fan and increasing the noise spectra.

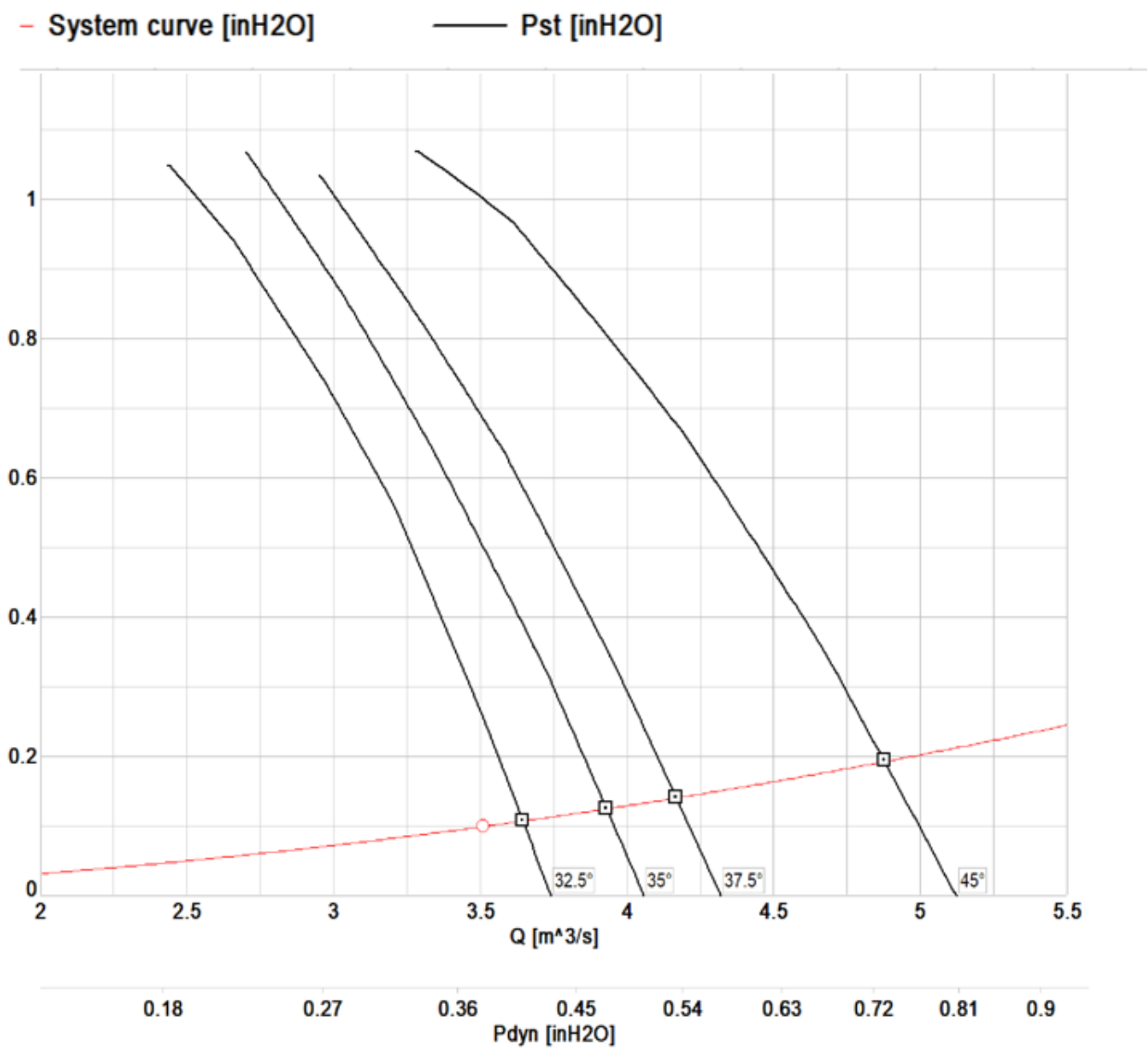


Figure 4.4: Performance and efficiency curves of M type blade at motor speed 1400rpm [50].

The materials considered for the blade were Aluminium, Glass Reinforced Polyamide (PAG), and Glass Reinforced Polypropylene (PPG). Aluminium has the highest Tensile Strength of 240 MPa compared to 165 MPa and 85 MPa for PAG and PPG, respectively [49]. Although Aluminium has superior strength and roughness ratings, it is also the most expensive.

PAG was chosen due to its credible price and strength and roughness , resulting in an impeller of 3.5kg. The hub is made from a die cast silumin alloy, produced by Hascon®.

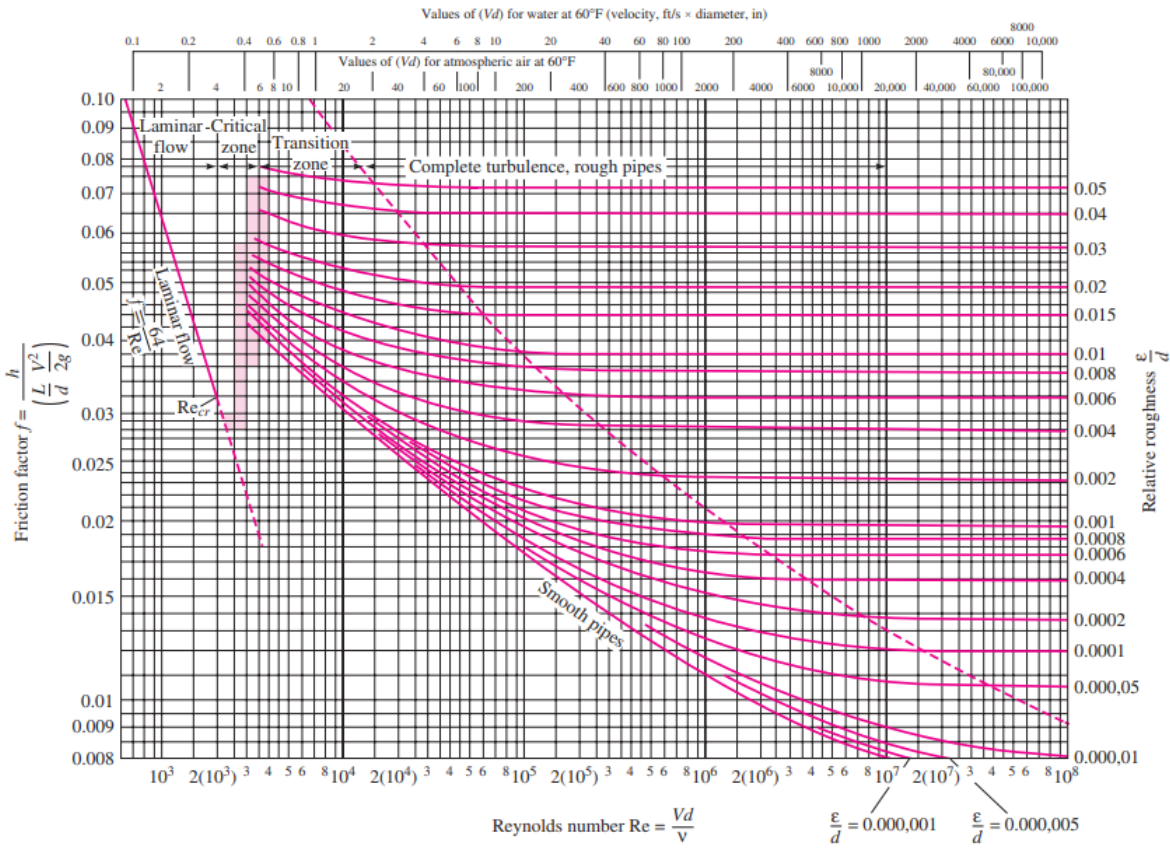


Figure 4.5: The Moody Chart for pipe friction with smooth and rough walls [36].

4.4 Stator

The stator, or guide vanes, improves the efficiency of the machine by regaining some static pressure. They reduce the whirl velocity resulting in smoother outlet airflow, important for a wind machine.

Stator design is less critical to the performance of the fan than the rotor. Phenomena such as boundary layer and separation are less pronounced. The stator will be manufactured using a single thickness Glass Reinforced Plastic (GRP) structure curved to redirect the flow. GRP was selected due to its credible roughness, material characteristics, and ease of manufacture. This reduces cost and allows Artem to manufacture the structure themselves.

The number of guide vanes should exceed the number of rotor blades. The risk of choking is remote and smaller distances between blades increases effectiveness. There should be no common

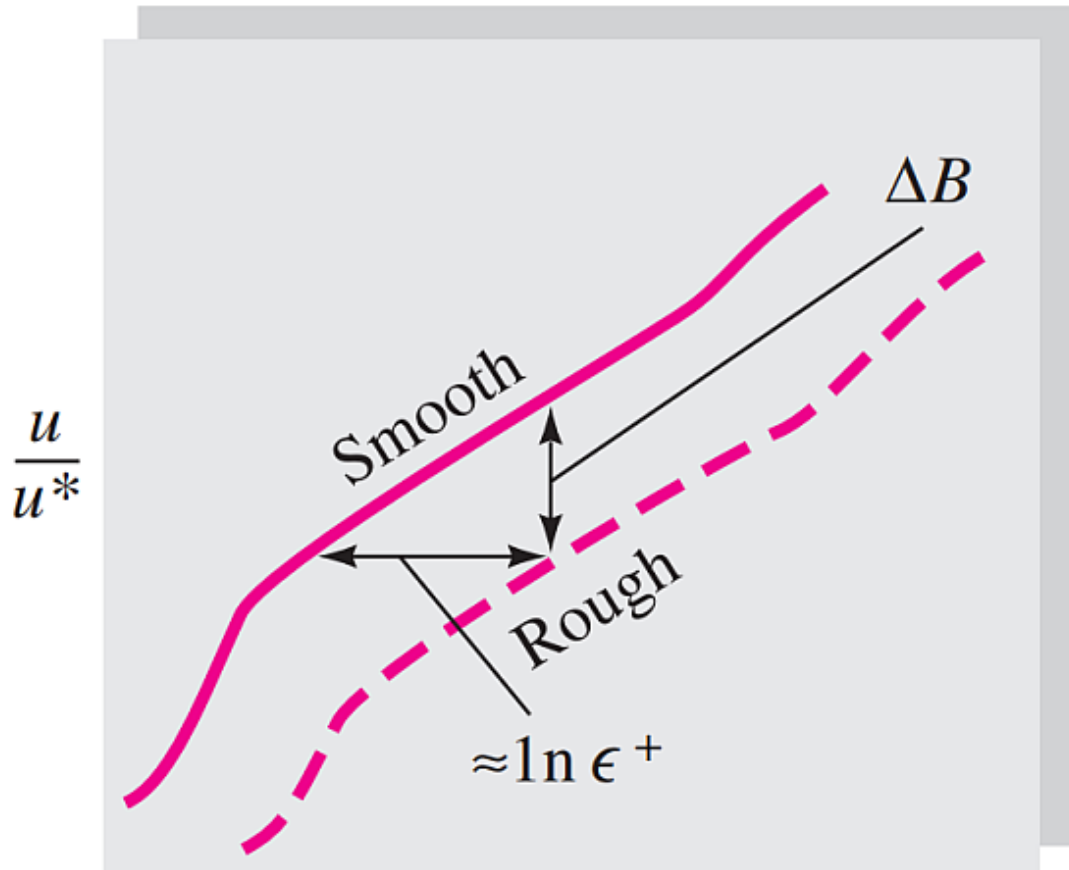


Figure 4.6: Logarithmic wall layer chart for smooth and rough walls [36].

divisor between the number of stators and rotors, to avoid two or more rotor and stator blades passing simultaneously, which causes higher peaks of noise fluctuation. Eleven guide vanes were chosen.

Inlet and outlet angles were calculated from velocity vectors of the flow, considering clockwise rotation of the impeller if looking into the inlet bell end of the duct (see Chapter 2). Stator inlet relative flow is $\beta_2 = 45^\circ$, assuming complete flow congruence of the blade. This is a crude assumption, and there is scope for further work to model the rotor exit flow more accurately. This is beyond this project and the approach is deemed acceptable for stator design.

The corresponding stator vane aims to axially align the flow. Calculations for the stator are shown in Appendix C. This resulted in guide vanes of camber 45° , and chord length of 136.5mm. The hub diameter is 200mm. The stator weighs 11kg.

There should be a clearance of 10% of the rotor diameter between the rotor and stator, a clearance of 60mm will be applied. [12].

4.5 Motor

Artem owned a motor of 2.2kW power, weighing 18kg, which reduced costs drastically. The most dominant criteria was the air flow capabilities of the machine. There was scope to adjust the motor if needed.

After calculations and checks of the chosen impeller, the motor was deemed acceptable, see Appendix A. Higher flow rates could be achieved with a higher power motor. A power of 3.5kW would deliver 52mph winds rather than 43mph. The cost of a new motor does not justify this.

4.6 Housing Design

A well designed fan housing, known as the duct or cowl, increases air flow, and reduces recirculation of air. Tip clearance should be kept to 1% of the rotor diameter. The tip clearance is 6mm. The inner diameter of the duct is 612mm, see Figure 4.7 [12].

The aerodynamically important aspects of the duct include tolerance, surface roughness and tip clearance. The duct must support the static, dynamic and pressure loads of the components it will support, i.e. the motor, rotor, stator and safety guards.

Aluminium, Steel and GRP were considered for the construction of the fan housing. Their properties are compared in Table 4.2. GRP was chosen due to its superior roughness coefficient to Steel and its favourable strength-to-weight ratio.

GRP is easily manufactured by Artem, offsetting higher raw material costs. The inlet bell and cowl can be constructed as one piece, reducing joints which can cause leakage and inefficiencies. GRP allows for the inclusion of aeroacoustic absorbent material in between the layers of GRP, which will help to absorb the noise and reduce the far-field sound generation.

4.6.1 Inlet Bell

Figure 4.8 demonstrates improved flow patterns obtained when the duct entrance is equipped with an inlet bell. Inlet bells reduce duct resistance and increase the efficiency of the fan. They can increase flow by approximately 15% [12].

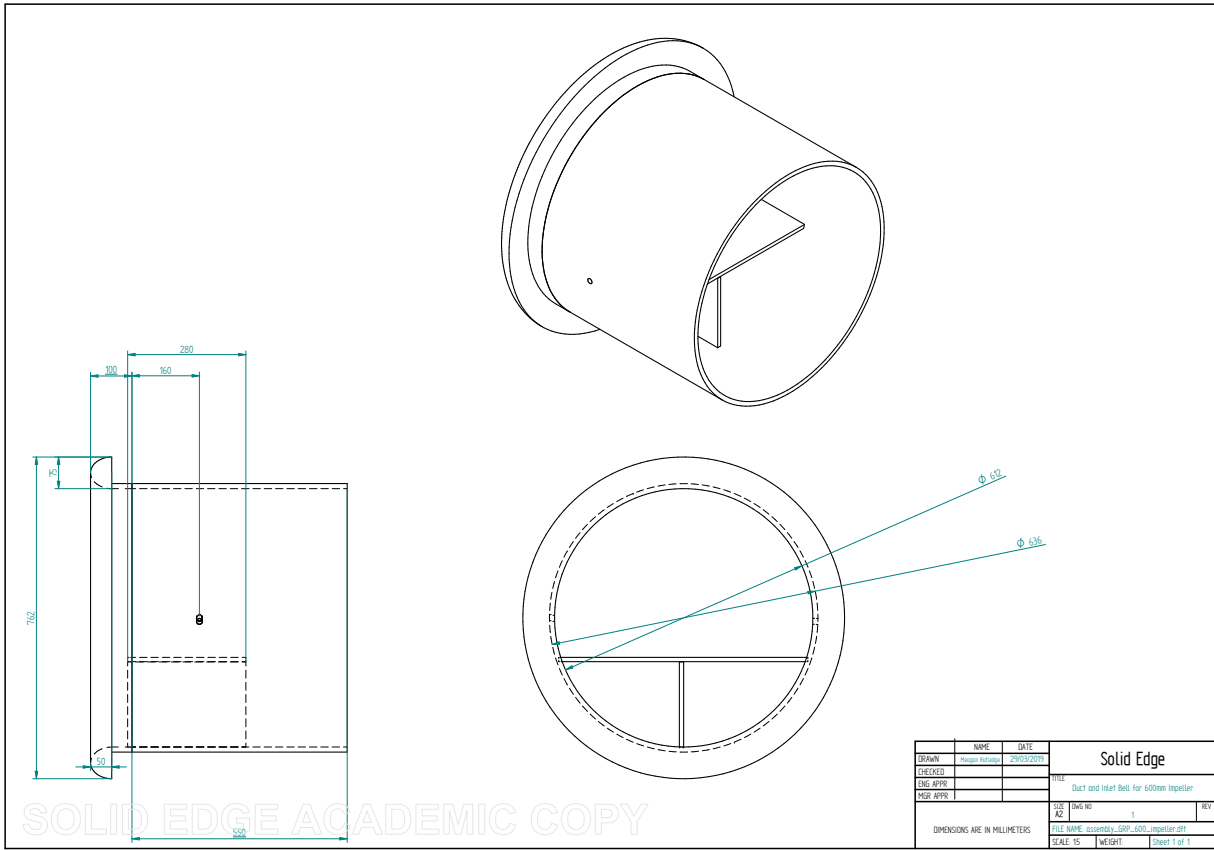


Figure 4.7: Dimensioned drawings of fan housing, created in Solid Edge® [58].

The profile can be modelled as a simple radius, aerofoil or ellipse. An elliptical profile provides the best aerodynamic performance and is easily manufactured. This profile is defined by dimensions a and b , see Figure 4.9. For optimum performance the ratio of a/b should be approximately 2.67 [51].

For the best results, the radius should be at least $r = 0.14D$, with r and D shown in Figure 4.8 [12]. This would result in diameters in excess of 800mm. The inlet was adapted to fit the brief while still maintaining some flow benefits.

Flow analysis was performed to assess the comparable flow performance of a minimised radius. Three different scenarios were considered: an inlet bell with dimension $a = 100\text{mm}$ and $b = 37.5\text{mm}$, to fit the door requirements and adhere to a ratio of 2.67; an inlet bell with the recommended radius of $0.14D$ which led to $a = 86\text{mm}$ and $b = 230\text{mm}$; and no inlet bell.

The flow was modelled using ANSYS®. The geometry was modelled as the air profile inside the housing. Meshing included an inflation of 15 layers at the wall to allow boundary layer analysis and a no-slip condition at the wall. The inlet and outlet air speed was 5.08m/s and 17.88m/s, respectively.

Figures 4.10, 4.11 & 4.12 show the surface shear stress, turbulent eddy frequency and turbulent kinetic energy of the different models, respectively. There is significant improvement through the use of an inlet bell. Higher turbulence depicted for no inlet bell is the result of boundary layer flow

Material	GRP	Aluminium	Steel
Volume [m^3]	0.0129	3.72×10^{-3}	2.64×10^{-3}
Density [$\frac{kg}{m^3}$]	1800	2700	7800
Weight [kg]	23	10	21
Tensile Strength [MPa]	35-150 depending on glass content	240	500
Absolute Roughness Coefficient, ϵ [mm]	0.0015	0.001	0.045-0.09
Cost [£/kg]	1.20	1.00	0.5

Table 4.2: Material Properties of GRP, Aluminium and Steel, data from [66]

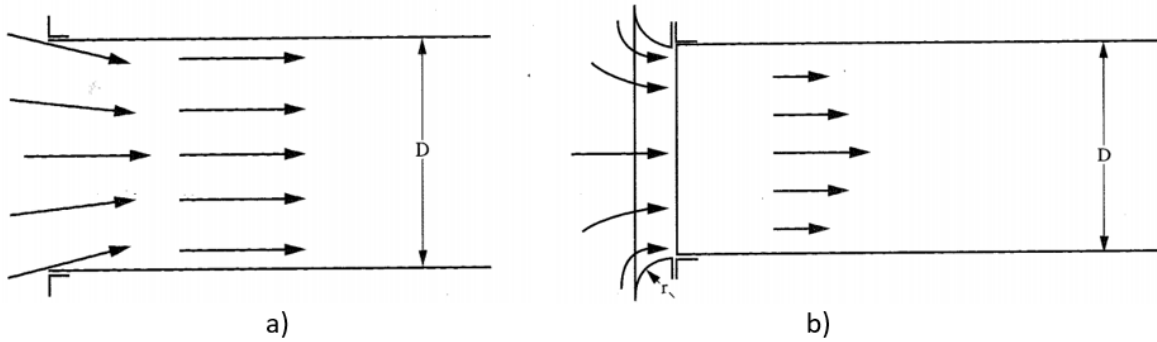


Figure 4.8: Air flow entering a) a round duct and b) a round duct with a venturi inlet at the duct entrance [12]

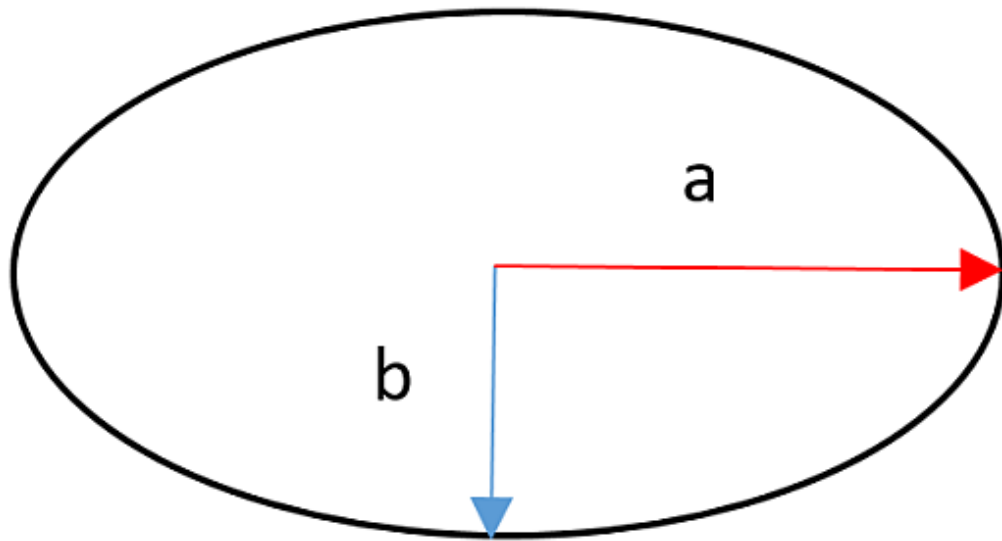


Figure 4.9: Schematic of an ellipse with labelled dimensions a & b.

and separation caused by the sharp housing inlet. This is likely to culminate in fan tip starvation of air.

Differences between the smaller inlet bell and the recommended dimensioned model are apparent. The surface shear stress of the larger inlet bell is minimised in comparison. This indicates smoother boundary layer flow. However, the smaller inlet bell improves the flow characteristics sufficiently and was ultimately adopted.

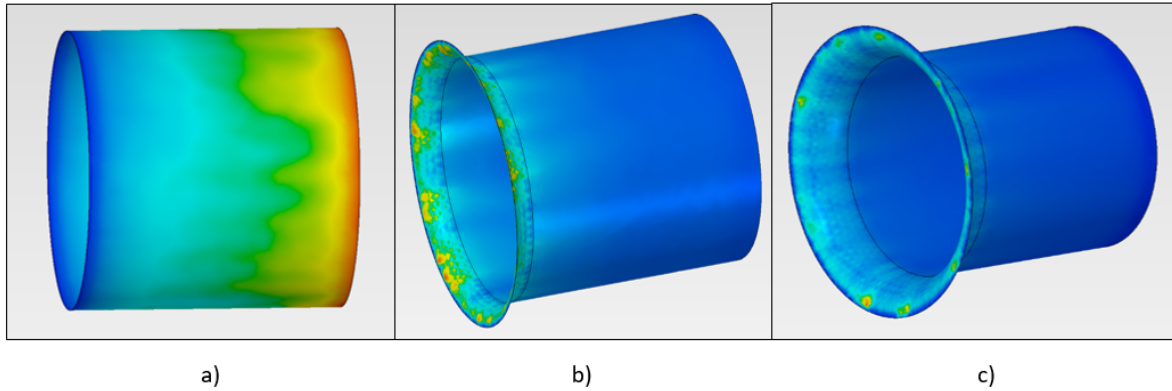


Figure 4.10: Surface Shear Stress Contour Depiction of a) no inlet bell b) inlet bell with elliptical profile $a=100\text{mm}$ and $b=37.5\text{mm}$ and c) inlet bell with elliptical profile $a=230\text{mm}$ and $b=86\text{mm}$ developed using ANSYS® [60]

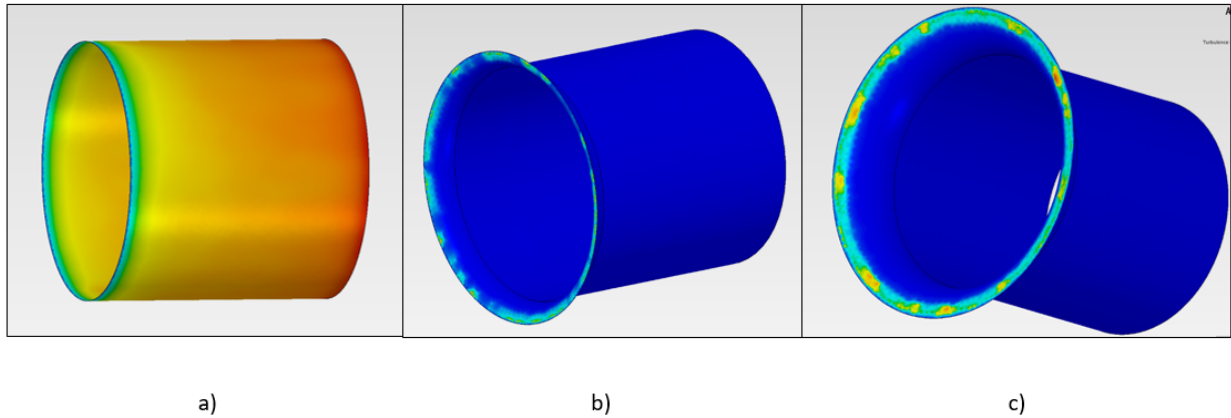


Figure 4.11: Turbulent Eddy Frequency Contour Depiction of a) no inlet bell b) inlet bell with elliptical profile $a=100\text{mm}$ and $b=37.5\text{mm}$ and c) inlet bell with elliptical profile $a=230\text{mm}$ and $b=86\text{mm}$ developed using ANSYS® [60]

4.6.2 Safety Guards

Safety Guards are required to protect operator's fingers as well as the rotor from large pieces of debris which may choke the system. There will be a safety guard on either end of the housing.

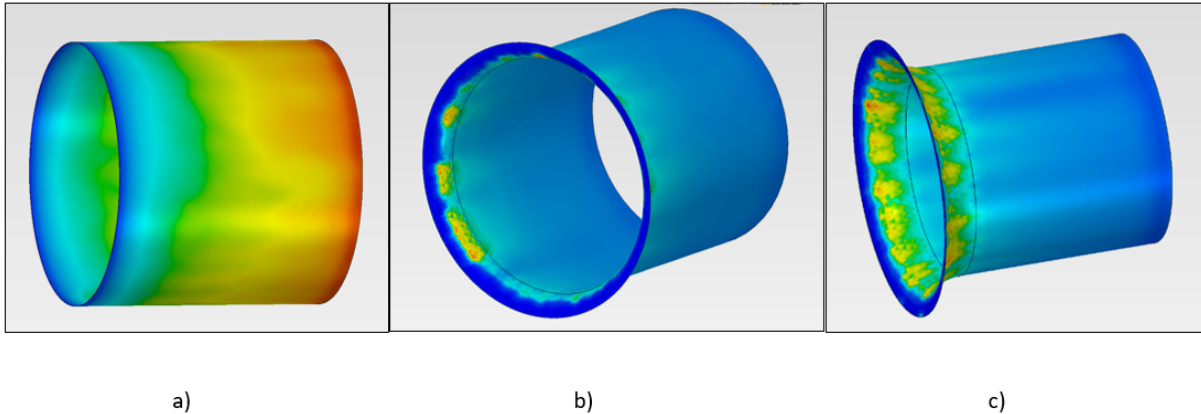


Figure 4.12: Turbulent Kinetic Energy Contour Depiction of a) no inlet bell b) inlet bell with elliptical profile $a=100\text{mm}$ and $b=37.5\text{mm}$ and c) inlet bell with elliptical profile $a=230\text{mm}$ and $b=86\text{mm}$ developed using ANSYS® [60].

4.7 Stand

The stand was designed for the dynamic and static loading of the machine, see Appendix F for calculations. The stand consists of a U-stand and rotating stand to allow for the pan and tilt of the machine.

The U-stand will be constructed from a mild steel bar ($8\times32\text{mm}$) bent into a U shape to support the fan. This will be connected to the housing through a moulded boss. An M10 bolt with a star knob will be used to secure the fixture, allowing fastening and unfastening for the adjustment of tilt. Bolts were chosen using bolt stress analysis, see Appendix D. The position of the U-stand relative to the fan housing is important for balancing the component forces. It will be placed 160mm from the duct inlet, as shown in Figure 4.7, see Appendix E.

Analysis on deflections and vibration modes were performed using Solid Edge® to ensure that the structure is sufficiently strong and to assess the natural frequency. These validated the design of the stand.

The U-stand will be connected to a rotating stand to allow the machine to be easily panned. Some rotating stands have been identified that will allow this, see Figure 4.13. This can be attached to the U-stand using M10 bolts, which the receiver is fitted with.

4.8 Modelling and Optimisation

The design was modelled to assess noise and vibrations. Noise generation is inherent to the fundamental operation of a fan, but excessive noise indicates inefficiencies and should be minimised. In the context of wind machines, noise is a main minimisation criteria.

Aerofoil blades, inlet bell and minimised tip clearance were implemented to limit noise. In order to assess any further mitigation, computational analysis was performed to predict noise mechanisms.

Mechanisms of noise include gear noise, bearing noise, aerodynamic noise and vibrational



Figure 4.13: Fan stand, allowing rotation, from Roger George Special Effects [67].

noise. The noise analysis focuses on aerodynamic and vibrational noise sources.

Vibration can impact the structural integrity of the system. High levels of noise can indicate resonance, a phenomenon which occurs when the forcing frequency matches that of the natural frequency of a structure or object. The result is a high displacement and amplitude of vibration. This causes large stresses and can vary in its effect from fatigue and wear to fatality.

4.8.1 Vibrations and Vibrational Noise

There are numerous vibrational noise mechanisms in a fan. Some of the most prominent causes are: unbalanced motors and rotor, interaction of natural frequencies and forcing frequencies, and loose fastenings.

Some of these are difficult to mitigate at this stage. For instance, the motor dynamic balance will need to be assessed once the machine is assembled. Loose fastenings are a consequence of the manufacturing stage, rather than design. This is fairly easy to adjust as most of the fixtures, e.g. bolts, will be easily accessible.

Modal analysis on Solid Edge was performed to compare natural frequencies of structural components to the forcing frequency, see Figures 4.15 and 4.14. The natural frequencies of the stand and cowl are 116Hz and 486Hz respectively, this is well outside the range of the motor and each other. This means that the risk of resonance is low.

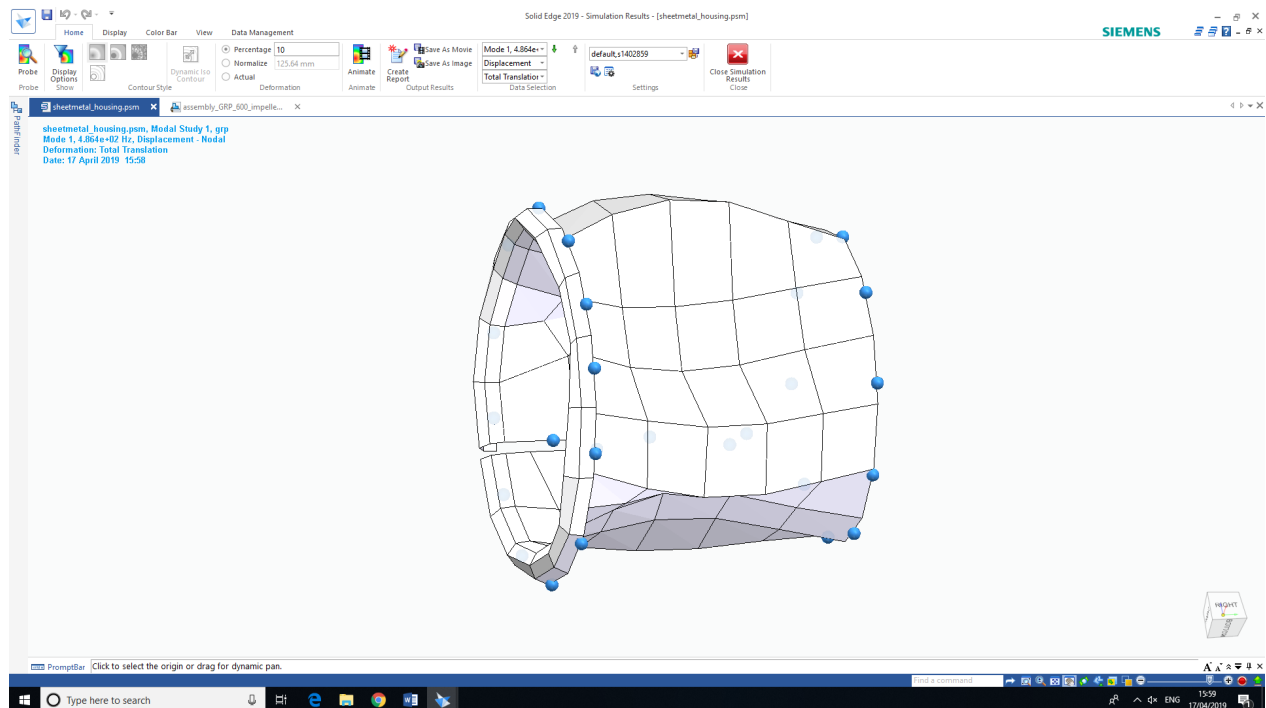


Figure 4.14: Cowl modal analysis in Solid Edge® [58].

Vibration noise can also occur near or at the stall region of a fan. The fan was selected to avoid the stalling range, as shown in Figure 4.4.

4.8.2 Aerodynamic Noise

The main generation mechanisms of aerodynamic noise are; turbulent inflow, self-noise (turbulent or laminar boundary layer, and boundary layer separation), trailing edge noise, secondary flows, and tip leakage related noise. This results in a noise spectrum which is broadband with superimposed tones of discrete frequencies, termed tonal noise. These noise sources can be described by elementary sources, e.g. monopoles, dipoles and quadrupoles [9]. The propagation and modelling of noise depends on its elementary definition.

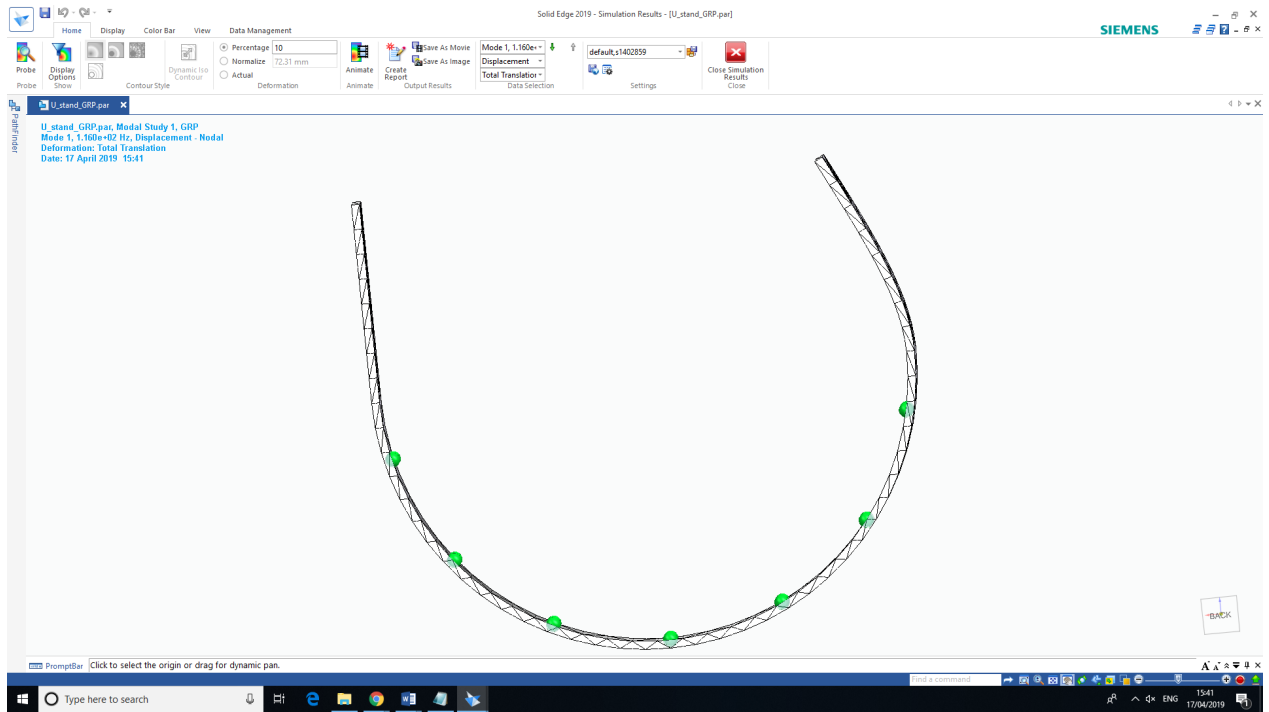


Figure 4.15: Stand Modal Analysis in Solid Edge

Monopole, Dipole and Quadrupole

The sound field of a monopole, dipole and quadrupole sources are shown in Figure 4.16. Many of the noise sources can cause both discrete and broadband noise, see Figure 4.17.

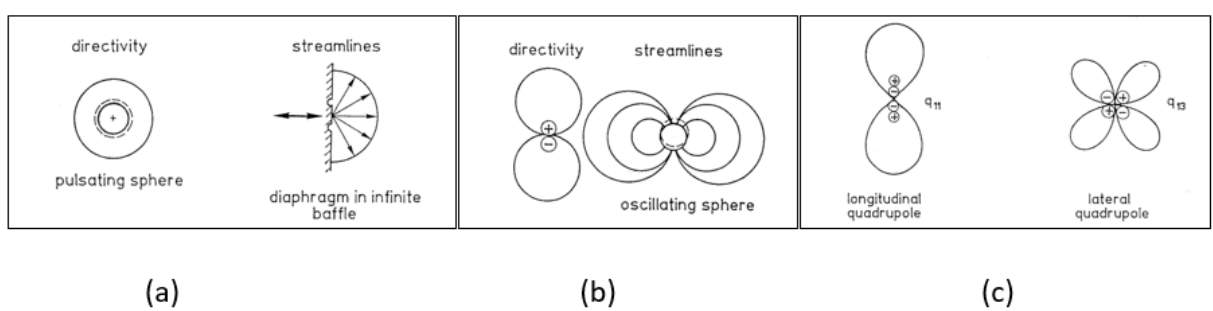


Figure 4.16: Directivity and streamline schematics for elementary noise sources; a) monopole b) dipole and c) quadrupole (adapted from [9]).

Tonal Noise

Tonal noise is caused by steady and unsteady aerodynamic forces. It is a consequence of: the fluctuating forces on the rotor blades, unsteady flow, turbulence, and nearby stationary objects (e.g. guide vanes, protecting guard). The spectrum of noise is discrete with spectral lines at the blade

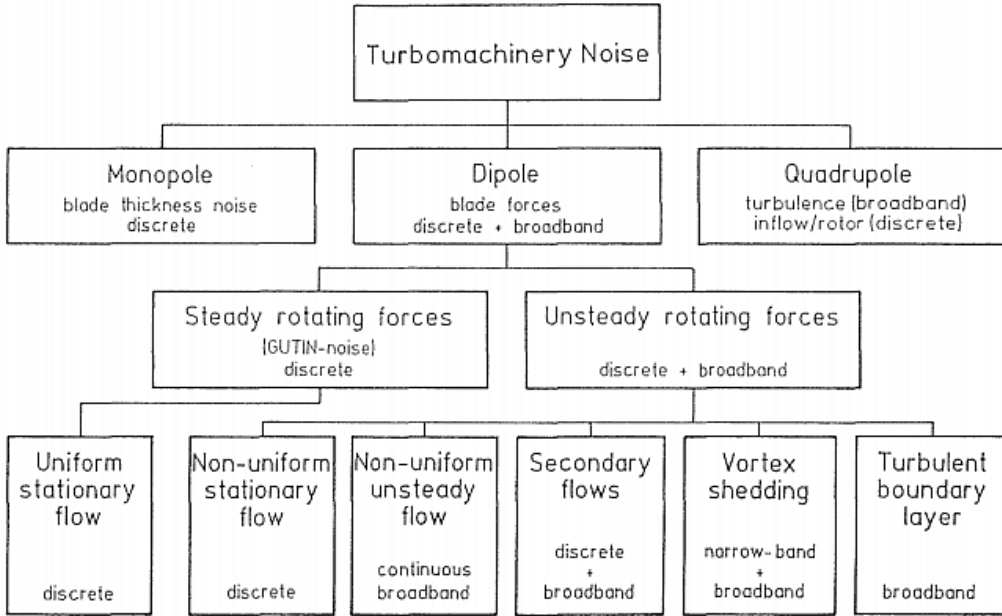


Figure 4.17: Summary of aeroacoustic source mechanisms relevant to turbomachinery noise [9].

passing frequency and its harmonics [9, 52].

Broadband Noise

Broadband noise is characterised by a continuous spectrum generated by random disturbances. It is caused by the interaction of turbulent flow with solid structures, including fan blades, guide vanes and duct structure. The most prevalent causes include: turbulent boundary layer noise, turbulence of inlet flow, vortex shedding, flow separation, tip vortex/clearance and stalled blade flow [52].

4.8.3 Modelling Aerodynamic Noise

Aeroacoustic prediction involves solving both sound generation and propagation [61].

There are at least three well-known methods to obtain a simulation of computing complex flow using Computational Fluid Dynamics (CFD) [53]:

1. Direct Numerical Simulation (DNS)
2. Large Eddy Simulation (LES)
3. Hybrid of Reynolds Averaged Navier Stokes (RANS) and LES

DNS provides accurate predictions. It requires a high grid resolution which makes it computationally expensive [53]. LES is less computationally demanding. The Sound Pressure Level

(SPL) can be obtained directly as part of the energy spectrum [52]. Difficulties include calculation of small turbulence vortices and the large velocity gradients at the initial boundary layer and near-field regions. Hybrid systems are formed by combining RANS and LES. Hybrid simulations usually adopt RANS calculations near the wall region and LES in the remaining regions.

The results from CFD must be used in accordance with an acoustic model in order to assess the noise generation and power of the system. Lighthill's equation was revolutionary to the combination of sound generation and propagation. This equation rearranges Navier-Stokes equation to an inhomogeneous wave equation, connecting fluid mechanics and acoustics. Acoustic analogy models include Ffowcs Williams and Hawkings (FWH) method, Amiet's theory, Acoustic Perturbation Equations and direct noise computation [61].

The FWH method is an extension to the Lighthill equation, given by eq. 4.3. Moving surfaces can be taken into account, making this approach suitable for turbomachinery prediction such as this analysis [62].

$$p'(x,t) = p'_Q(x,t) + p'_F(x,t) + p'_M(x,t) \\ = \frac{1}{4\pi} \frac{\partial^2}{\partial x_i \partial x_j} \int_V \frac{T_{ij}}{|r - r_0|} dV(r_0) - \frac{1}{4\pi} \frac{\partial}{\partial x_i} \int_S \frac{[p_{ij}]}{|r - r_0|} dS(r_0) + \frac{\rho_0}{4\pi} \frac{\partial}{\partial t} \int_S \frac{[v_i]}{|r - r_0|} l_i dS(r_0) \quad (4.3)$$

where T_{ij} is Lighthill's stress tensor, p_{ij} is a compressive stress tensor, ρ_0 is the fluid density at equilibrium, r is the observation point, r_0 the source point and v_i is the velocity of the surface [68, 69].

The acoustic pressure, p' , is the sum of the acoustic pressures arising from the different sources; monopoles (third term of eq.4.3), dipoles (second term) and quadrupoles (first term). For low Ma quadrupole contribution is small compared to mono- and dipoles and for computational reasons is omitted from noise analysis operations. The FWH is easily coupled with CFD results and is less computationally expensive than other models. ANSYS FLUENT®, as used for these noise predictions, utilises FWH along with RANS and LES approaches.

The CAD model of the rotor and housing was imported from Solid Edge®. The stator was not included as it caused the analysis to be too computationally expensive. The stator does have a significant impact on the noise generation, undermining the acoustic prediction.

A mesh of 2,177,864 elements was used with inflation at the fan housing surface. Minimal orthogonal quality of more than 0.1 and a max skewness of 0.9 is essential for an accurate mesh [64]. The mesh produced had minimum orthogonality of 0.14278, and an average of 0.83416. The maximum skewness was 0.9, and the average 0.27622. It was decided this was adequate. Figures 4.18& 4.19 show quality checking.

Boundary conditions for the RANS and LES calculation included inlet and outlet ambient pressure conditions, and no-slip walls. The rotation was simulated using the sliding mesh method. $k - \epsilon$ turbulence model with wall treatment was applied.

Issues arose with obtaining a final solution. These were caused by the complicated geometry of the rotor and meshing limits applied to ANSYS Student®.

The noise predictions were isolated to broadband noise. Peak noise was modelled at the blade tips producing 134 dB, see Figure 4.20. The fan is predicted to produce an average of 84.5 dB at the rotor exit. This is in agreement with common values for axial fans and superior to those

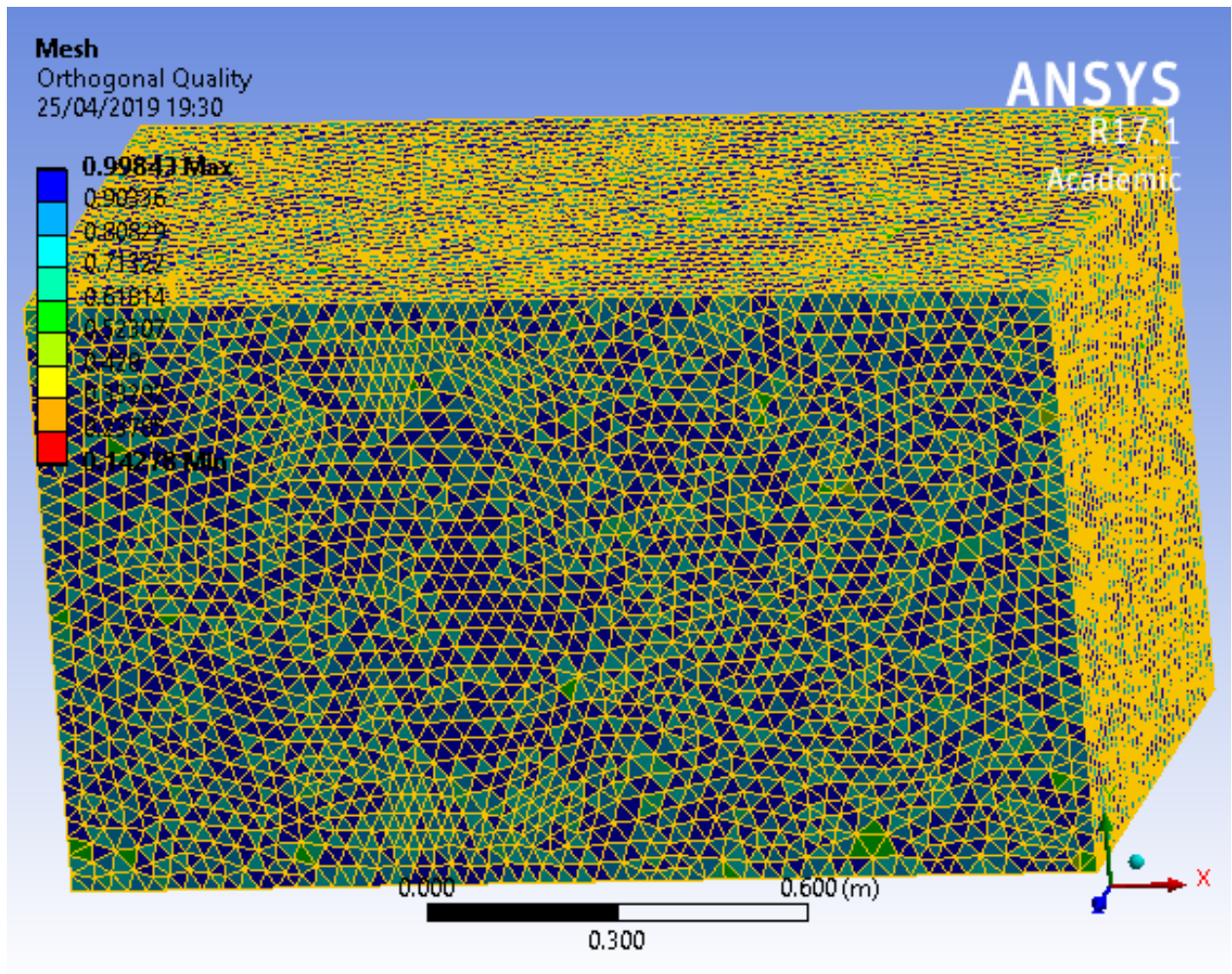


Figure 4.18: Orthogonal Quality Checking of Mesh in Ansys®

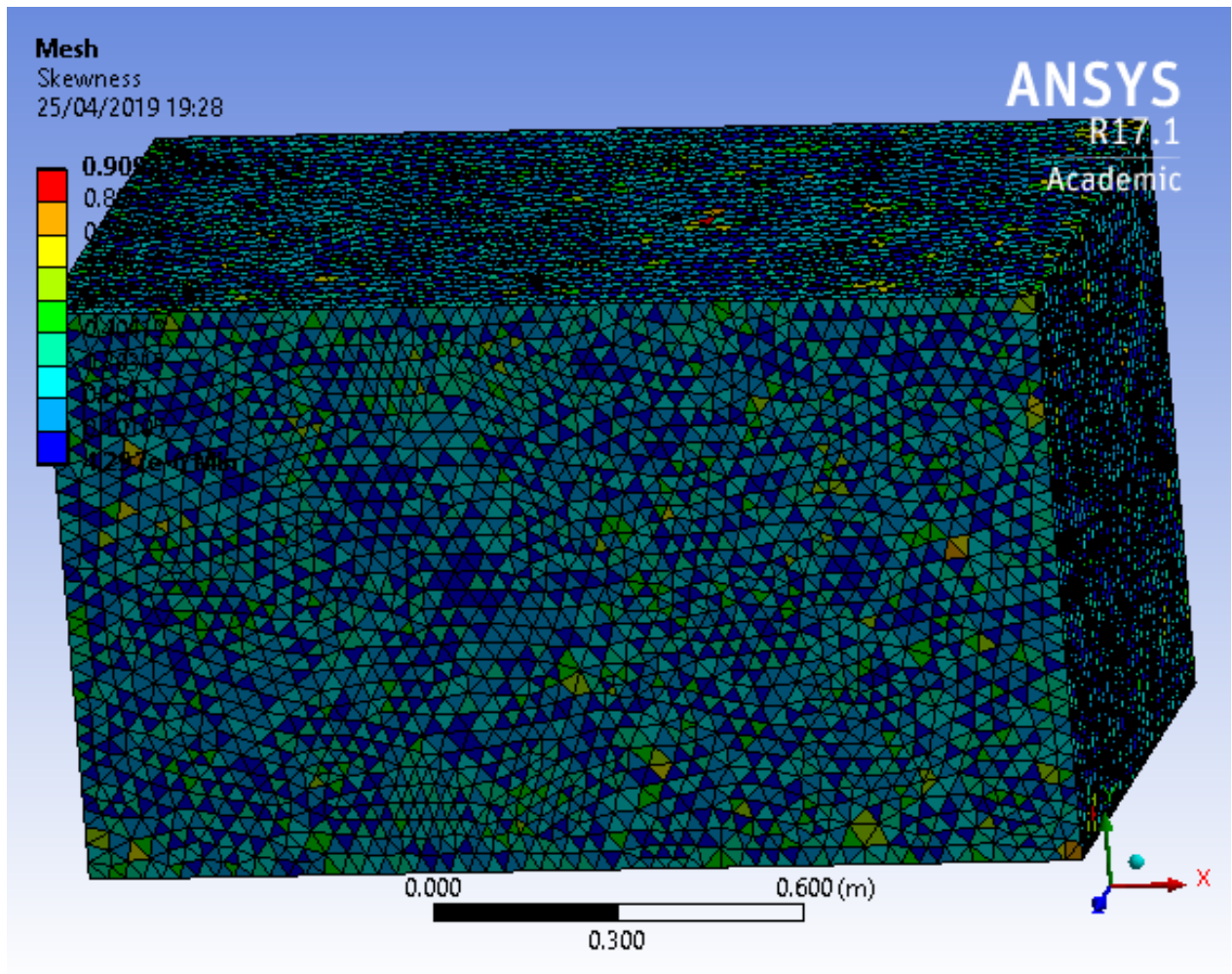


Figure 4.19: Skewness Quality Checking of Mesh in Ansys®

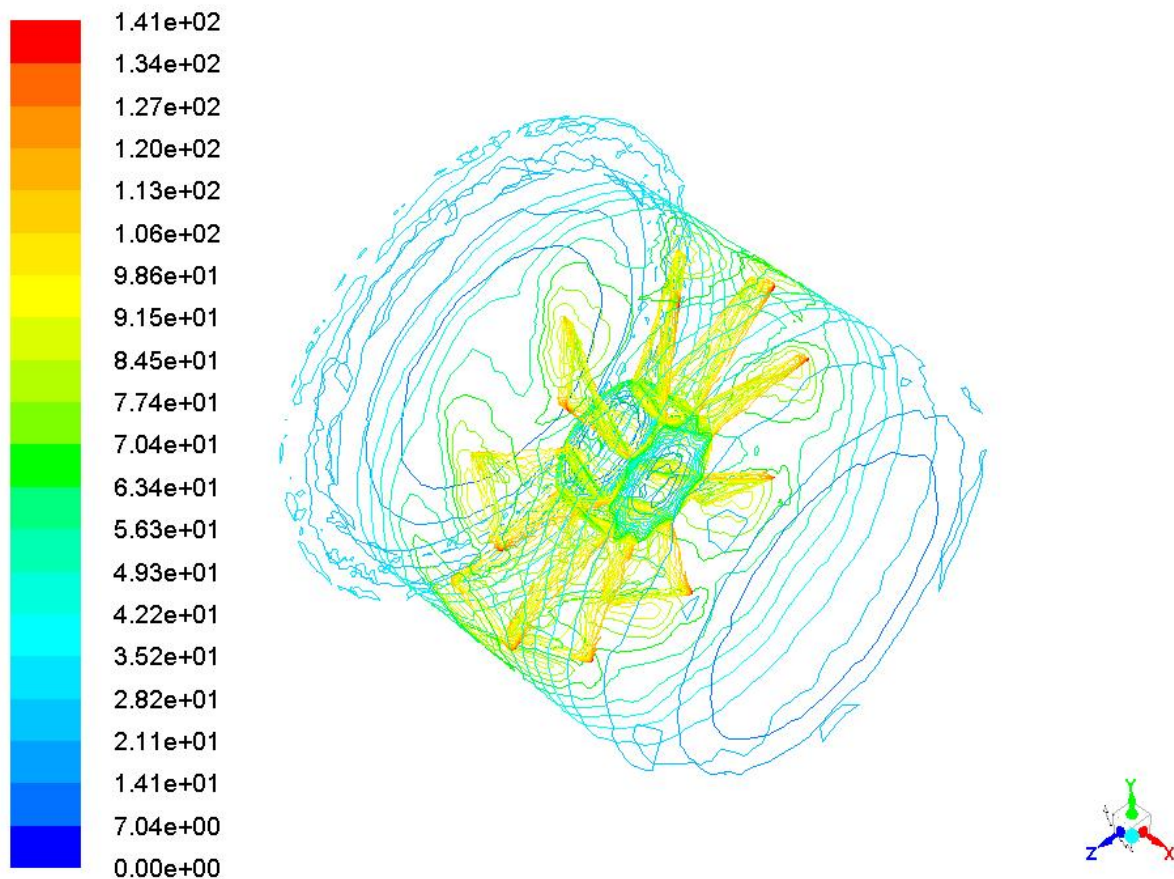


Figure 4.20: Contour Display of Broadband Acoustic Analysis in Ansys®

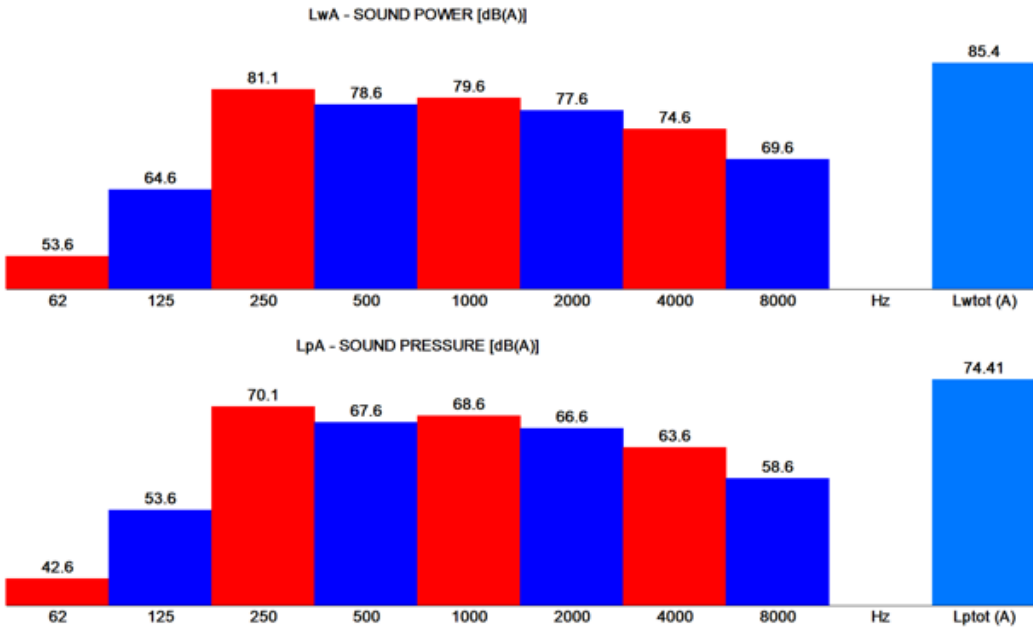


Figure 4.21: Sound power and pressure bar chart for M blade impeller from Qualyfan [50].

predicted by Hascon of 85.4 dB(A), see Figure 4.21 [72]. dB(A) is the relative sound as perceived by the human ear, it is tailored to frequencies accordingly and is less than the total value. The lower predicted noise power of the designed fan suggests that the shroud tip clearance and inlet bell improve flow. The validity of this is questionable due to the omission of tonal noise. Further predictions are needed, however some value can be taken from this analysis.

Broadband noise is arguably more relevant for design feedback. It represents the effect of the inlet bell, blade type, and tip clearance. Although tonal noise is important for the rotor/stator interaction the stator was already omitted from the mesh so this becomes obsolete.

Through the use of acoustic absorbent lining between layers of GRP, some of this broadband noise may be diffused, giving the wind machine a better noise performance. The tip clearance can be concluded as optimal by the relatively low noise level at the fan housing near the tip blades, suggesting minimal recirculation.

Chapter 5

Manufacturing

The GRP housing, along with the inlet bell, is manufactured using moulds which the GRP is placed into. The patterns are created from a Polyurethane (PU) tooling board machined using a CNC machine to build layers of 100mm thickness. The layers are then assembled, sanded and primed to create a unified surface. During this stage a relief of Artems logo can be 3D printed. This allows for the personalisation of the machine, see Figure 5.1.

A laquering can be applied to tint the fibreglass so that a pre-coloured and smooth surface can be removed from the mould, both for aerodynamic purposes and appearance. The parts are then moulded. In order to release the mould pieces it may need to be split, creating seams. The placement of these seams is important for reducing post-processing and the structural integrity of the object. The stator will be manufactured using the same procedure.

5.1 Assembly

The stator will be assembled to the housing through slits in the GRP housing, the stator can then be bolted to the fan housing. The motor shaft has a keyway of dimensions shown in Figure 5.2. The hub will be machined with the corresponding key to allow the two parts to fit together.

The motor will be bolted to a motor stand made of steel which is bolted to the fan housing, using M8 bolts. The motor stand will be 210mm high to ensure the centre of the motor shaft coincides with the centre of the housing.

The fan housing, with its constituent parts, will be fixed using M10 bolts to the U-stand, which is in turn assembled on the rotating stand.



Figure 5.1: GRP Part for bell-inlet with Artem logo relief

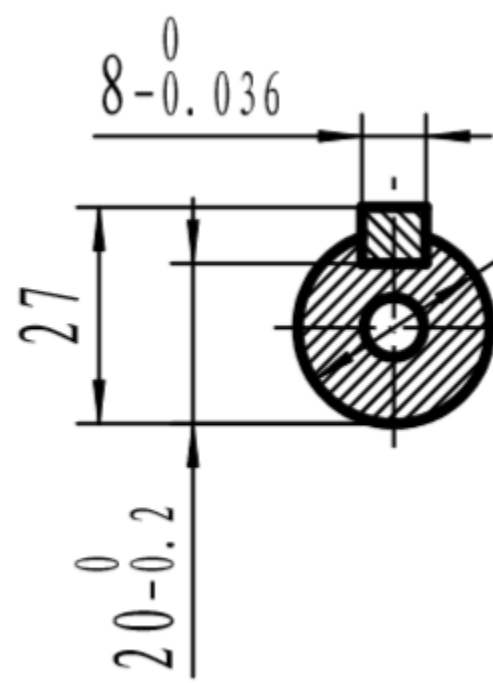


Figure 5.2: Motor keyway dimension [71]

Chapter 6

Discussion

The design strategy and outcomes will be discussed in order to assess their success in relation to the project objectives set out in Chapter 1.

6.1 Evaluation of Design

With regards to Table 1.1, the design process succeeded in achieving an easily manufacturable machine fulfilling the main requirements of wind speed, tilt and pan, and weight restrictions. The final product weighs 63kg, has a largest width of 762mm and will produce wind speeds of around 43mph. The actual wind speed will be affected by friction losses along the housing, and rotor/stator interactions.

Simple and effective design criteria were optimised to produce a machine of good operation within cost, time and size constraints. The film and TV context emphasised the need for ease of manufacturing, low noise levels, and effective airflow output.

Whilst fan design is considered tried and tested technology, it is also difficult to design a particularly good fan. The aim was to optimise the efficiency of the fan by focusing on the important criteria for aerodynamic performance. No physical testing has been possible and analysis relies on performance curves supplied by Hascon® and simulations performed on Solid Edge® and ANSYS®. The fan is evaluated as per its predicted performance, which undermines the analysis. Testing is beyond the time-scale of this project and further work is needed to assess the design practically.

A set of simple rules were outlined in order to ensure the adequate aerodynamics of the system. These included: a tip clearances of 1% of impeller diameter, material selection for low roughness, an inlet bell of elliptical profile, and outlet guide vanes. They are applicable to a machine of any size and could be applied in a program for future, somewhat automated design.

Solid Edge® was invaluable to successfully communicating design intent to Artem through 3D CAD models as well as dimensional drawings.

6.2 Evaluation of Noise and Vibration Modelling

6.2.1 Acoustic Modelling

Acoustic modelling is an experimental and difficult field, many different models exist because there is no precise solution. Limitations are associated with the methods involved for approximating the flow conditions. For instance, LES is not suited to trailing noise modelling [65]. Similarly, RANS has drawbacks in transition modelling and is unable to accurately model separation. The hybrid approach, adopted by ANSYS®, aims to mitigate these errors by employing RANS for high Re areas and LES for boundary flow. However, issues can arise with the LES-RANS interface, resulting in inaccuracies [63].

LES is a filtration method which computes the size of the eddies in a flow and filters out the smallest scales, on the basis that large eddies have more energy than smaller ones so will have a bigger impact on noise generation. Mesh width is regarded as an appropriate filter size, explaining the importance of mesh treatment. This model was significantly restricted in mesh size, directly impacting LES and RANS calculations and reducing the reliability of the predictions.

Significant noise generation is caused by stator/rotor interaction. This model did not include the guide vanes meaning that noise is likely to be underestimated. The effect of the blade and housing roughness were also not included. Both of these materials were chosen for their low level of roughness so these effects are expected to be minimal.

The tonal noise predictions failed due to the meshing procedure and computational expense of the system. This significantly reduces the validity of the results. However, the model did predict broadband noise levels similar to other axial fans and within range of values given by Hascon®. The results are certainly not null. They demonstrate some of the main noise mechanisms of the machine, and indicate good tip clearance.

6.2.2 Modal Analysis

Most noise, vibration or failure problems in mechanical systems are caused by excessive dynamic behaviour. This behaviour results from complex interactions between applied forces and the mass-elastic properties of the structure. Finite Element Modeling (FEM) is a highly useful tool for structure dynamic analysis. Solid Edge®, due to its modelling and mesh capabilities, make it very suited to such analysis.

This modal analysis did not take into account the entire structure, but merely the mechanisms that were predicted to cause particularly harmful vibrations. The models were simplified in order to carry out this analysis. They are a prediction but not a guaranteed assurance that the system is protected from resonance. The analysis provided a good indicator that the fan housing and stand have natural frequencies out of the range of the forcing frequency. It was therefore not necessary to mitigate against the risk of resonance.

6.3 Comparison of Project to Objectives

Most of the six objectives outlined in the introduction have been fulfilled to varying degrees.

Key engineering concepts relevant to the wind machine system were explored through a rigorous literature and mathematical review, outlined in Chapters 2 & 3. Guidelines and ideas from this were applied to the design phase. Solid Edge® and ANSYS® were utilised to perform noise, stress and vibration analysis on the wind machine design. Inlet flow characteristic were modelled for different bell inlet radii in order to determine their effect.

The design was optimised according to size and cost, whereby design decisions were based on limiting cost whilst achieving superior aerodynamic performance. Each design criteria (e.g. rotor, housing, etc.) were optimised individually and their collective design was evaluated. More in depth optimisation could have included CFD simulations of the entire flow to adjust the geometry and evaluate the differences, as well as comparison to more design ideas, as most of the designs were varying sizes of a similar design.

The success of the machine was assessed theoretically. It was evaluated against the design requirements and it was determined that it fulfilled them adequately. Due to time constraint, no physical analysis of the working machine was performed which limits its assessment.

Issues arose with time delays, despite mitigation of these in the original project planning, see Appendix G. Despite this, most of the project objectives were achieved.

Chapter 7

Conclusions and Further Work

7.1 Conclusion

This project successfully implemented a design strategy for a wind machine for use on television and film sets. Following extensive research and mathematical analysis, the most important phenomenon highlighted were: the transfer of shaft work to the air, the boundary layer flow and separation. Great care has been taken, within the context of the entertainment industry, to avoid over-engineering of the design. The key design parameters were identified as the rotor, stator, housing, motor and stand. These were focused on for simple and effective improvements, including material selection and tip clearance. The final design was 762mm at its largest width, weighs 63 kg, produces wind speeds of approximately 43mph and has tilt and pan capabilities and therefore fulfills the requirements set out in the brief.

The project involved CFD simulations using ANSYS® to predict the aeroacoustics of the system, and Solid Edge® to model the designs and evaluate vibrations which may occur causing structural instabilities. The design was assessed as structurally stable. No physical testing has been done on the final machine to assess its practical performance.

7.2 Further Work

There are a number of ways in which this project could be continued. In particular testing of the machine to more accurately assess its relative successes and short comings. The tests should include wind speed and area of effect, and noise analysis of the system. Noise analysis should be undertaken with care to avoid propagation of noise from surrounding objects in order to measure the noise mechanisms from the machine itself, as was modelled. This can also be used to validate the noise prediction method carried out on ANSYS®.

Further work could include CFD analysis in order to design the rotors and stators. However, within the context this is perhaps unrealistic.

The use of wind machines means many external mechanisms may occur which will increase the noise and decrease the performance of the fan. For example, the machine may be operated outside in conditions of strong cross-flow. This causes non-uniform velocity profiles at the inlet and will increase noise mechanisms such as forces on blades. Further work could include protection from this.

It may be possible to set up a MATLAB® or Python code which automates the design process, predicting size and power requirements and incorporating the set of design ‘rules’ discovered throughout this project. This includes tip clearance, axial clearance between components and inlet bell dimensions. If the material is specified the corresponding housing thickness and dimensions required could be calculated. This would reduce the time for designing new wind machines significantly, leaving Artem to cater to their clients project proposals.

References

- [1] Artem. "*Artem Case Studies: London 2012 Olympic Ceremonies*". 2012. URL: <https://www.artem.com/portfolio/571> (visited on 10/02/2019).
- [2] BBC News. "*How the London 2012 Paralympic Ceremonies were made*". 2018. URL: <https://www.bbc.co.uk/news/uk-england-london-45297769> (visited on 10/02/2019).
- [3] S Castegnaro. "Aerodynamic Design of Low-Speed Axial-Flow Fans: A Historical Overview". In: (2018), pp. 1–17.
- [4] W Rankine. "On the Mechanical Principles of the Action of Propellers". In: *Transactions of the Institution of Naval Architects* 6 (1865), pp. 13–39.
- [5] R. E. Froude. "On the part played in propulsion by differences of fluid pressure". In: *Transactions of the Institute of Naval Architects* 30 (1889), pp. 390–405.
- [6] M. Okulov, J. N. Sorensen, and G. A. M. Van Kuik. "Development of the optimum rotor theories". In: (2013).
- [7] N. E. Joukowsky. "Vortex Theory of Screw Propeller". In: *Trudy Otdeleniya Fizicheskikh Nauk Obshchestva Lubitelei Estestvoznaniya* 16 (1912-1915), pp. 2–31, 1–33, 1–23.
- [8] A Betz. "The theory of the Screw Propeller". In: *NACA Technical Notes* 83 (1921), pp. 1–19.
- [9] W. Neise and U. Michel. "Aerodynamic Noise of Turbomachines". In: (1994).
- [10] H. B. Urbach. "Differential Forms of Euler's Turbo-Macginery Equation". In: (1989).
- [11] M. Borg. "ThermoFluids 3: Turbomachinery Notes". In: The University of Edinburgh, 2018.
- [12] F. B. Bleier. *Fan Handbook: Selection, Application and Design*. McGraw-Hill, 1997.
- [13] P. Ryden. "Investigations of Single-Stage Axial Flow Fans". In: (1937).
- [14] R. A. Wallis. "Axial Flow Fans: Design and Practice". In: (1961).
- [15] L. C. Mansson and S. H. Traberg-Larsen. "Flow Characteristics of the Dyson Air Multiplier". In: (2014).
- [16] P. Fernandez. "*Dyson's Air Multiplier with STAR-CCM+*". 2013. URL: <http://theansweris27.com/dysons-air-multiplier-with-star-ccm/> (visited on 08/02/2019).
- [17] J. Strickland and N. Chandler. "*How the Dyson Bladeless Fan Works*". 2014. URL: <https://electronics.howstuffworks.com/gadgets/home/dyson-bladeless-fan.htm> (visited on 08/02/2019).
- [18] You Me Patent & Law Firm. "*All the counterfeits of 'Jung Yong Jin Fan' kick out thanks to 'Super Patent'*". 2012. URL: http://www.youme.com/2005/en/nw2_30.asp (visited on 08/02/2019).

- [19] S. J. Van Der Spuy. “The design of a low-noise rotor-only axial flow fan series”. In: (1997).
- [20] R. M. Bass. “Factors Influencing the Aerodynamic Design of Low Pressure Axial Fans”. In: *Industrial Fans - Aerodynamic Design* (1987).
- [21] T. W. Smith. “A Practical Approach to the Design of Axial and Mixed Flow Fans”. In: *Industrial Fans - Aerodynamic Design* (1987).
- [22] S. Bianchi, A. Corsini, and A. G. Sheard. “Experimental Characterisation of the Far-Field Noise in Axial Fans Fitted with Shaped Tip End-Plates”. In: (2012).
- [23] C. L. Morfey. “Amplification of Aerodynamic Noise by Convected Flow Inhomogeneities”. In: *Journal of Sound and Vibration* 31 (1973), pp. 391–397.
- [24] N. A. Cumpsty, F. E. Marble, and W. R. Hawthorne. “The interaction of entropy fluctuations with turbine blade rows; a mechanism of turbojet engine noise”. In: *Proceedings of the Royal Society* 357 (1977), pp. 323–344.
- [25] S. C. Bradwell. “Standard, Quiet and Super Quiet - The Modelling of Flow and the Reduction of Turbulences”. In: (unknown).
- [26] T. Fukano, Y. Takamatsu, and Y. Kodama. In: *Journal of Sound and Vibration* 111 (1989), pp. 250–256.
- [27] M. Inoue and M. Kuroumaru. “Structure of Tip Clearance Flow in an Isolated Axial Compressor Rotor”. In: *Journal of Turbomachinery* 113 (1991), pp. 252–259.
- [28] J. A. Storer and N. A. Cumpsty. “Tip Leakage in Axial Compressors”. In: *Journal of Turbomachinery* 117 (1995), pp. 336–347.
- [29] B. Lakshminarayana, M. Zaccaria, and B. Marathe. “The Structure of Tip Clearance Flow in Axial Flow Compressors”. In: *Journal of Turbomachinery* 117 (1995), pp. 336–347.
- [30] S. Bianchi, A. Corsini, and A. G. Sheard. “Synergistic Noise-By-Flow Control DDesign of Blade Tip in Axial Fans: Experimental Investigation”. In: *Noise Control, Reduction and Cancellation Solutions in Engineering* (2012).
- [31] B. D. Mudridge and C. L. Morfey. “Sources of Noise in Axial Flow Fan”. In: *Journal of the Acoustical Society of America* 51 (1972), pp. 1411–1426.
- [32] R.E. Longhouse. “Control of Tip-Vortex Noise of Axial Flow Fans Operating at Design and Off-Design Conditions”. In: *Journal of Sound and Vibration* 58 (1978), pp. 201–214.
- [33] T. Fukano and C. M. Jang. “Tip Clearance Noise of Axial Flow Fans Operating at Design and Off-Design Conditions”. In: *Journal of Sound and Vibration* 275 (2004), pp. 1027–1050.
- [34] F. Kameier and W. Neise. “Rotating Blade Flow Instability as a Source of Noise in Axial Turbomachines”. In: *Journal of Sound and Vibration* 203 (1997), pp. 833–853.
- [35] A. Corsini, F. Rispoli, and A. G. Sheard. “Development of Improved Blade Tip Endplate Concepts for Low-Noise Operation in Industrial Fans”. In: *IMechE Power and Energy* 221 (2007), pp. 669–681.
- [36] F. M. White. *Fluid Mechanics*. 7th ed. McGraw-Hill, 2010.
- [37] T. Heinemann. “Axial Fans Under the Influence of Various Uniform Ambient Flow Fields”. In: (2017).

- [38] D. B. Ebin. “The Motion of Slightly Compressible Fluids Viewed as a Motion With Strong Constraining Force”. In: (1977), pp. 141–200.
- [39] S. Klainerman and A. Majda. “Singular Limits of Quasilinear Hyperbolic Systems with Large Parameters and the Incompressible Limit of Compressibility”. In: (1981), pp. 481–524.
- [40] S. Klainerman and A. Majda. “Compressible and Incompressible Fluids”. In: *Communications on Pure and Applied Mathematics* (1982).
- [41] T. Hagstrom and J. Lorenz. “On the Stability of Approximate Solutions”. In: (2002).
- [42] “Aerodynamic Fan Design - Computer Techniques”. In: *Industrial Fans - Aerodynamic Design* (1987).
- [43] R. Manufacturing. ”*Centrifugal Blowers*”. 2019. URL: <https://www.republic-mfg.com/blowers/centrifugal-blowers.asp> (visited on 10/02/2019).
- [44] Inc. Advanced Thermal Solutions. “Performance Difference Between Fans and Blowers and Their Implementation”. In: (2009).
- [45] S. L. Dixon and C. A. Hall. “Fluid Mechanics and Thermodynamics of Turbomachinery”. In: (2010), pp. 217–263. DOI: <https://doi.org/10.1016/B978-1-85617-793-1.00007-9>.
- [46] Department for Communities and Local Government. “Housing Standards Review”. In: (2013).
- [47] M. Wilkinson. “The Design of an Axial Flow Fan for Air-Cooled Heat Exchanger Applications”. In: (2017).
- [48] S. L. Dixon. “Fluid Mechanics, Thermodynamics of Turbomachinery”. In: (1998).
- [49] HasconWing®. “Fixed or Variable Airfoil Profile Axial Impellers”. In: (2012).
- [50] HasconWing®. *Qualyfan Selection Software*. Version 1.1. Mar. 17, 2019. URL: www.hwventilation.it.
- [51] B. Cory. “Fans and Ventilation”. In: (2005), pp. 43–75. DOI: doi.org/10.1016/B978-008044626-4/50005-X.
- [52] H. M. Atassi and M. M. Logue. “Modelling Tonal and Broadband Interaction Noise”. In: *IUTAM Symposium on Computational Aero-Acoustics for Aircraft Noise Prediction 6* (2010), pp. 214–223. DOI: doi.org/10.1016/j.proeng.2010.09.023.
- [53] A. Truong and D. Papamoschou. “Harmonic and Broadband Separation of Noise from a Small Ducted Fan”. In: (2015).
- [54] P. Kundu, I. Cohen, and D. Dowling. “Fluid Mechanics”. In: (2016).
- [55] S. Van Der Spuy and T Backstrom. “Performance of low noise fans in power plant air cooled steam condensers”. In: *Noise Control Engineering Journal* (2009).
- [56] U. Jaiswal and S. Joshi. “Design and Analysis of Stator, Rotor and Blades of the Axial flow Compressor”. In: *International Journal of Engineering Development and Research* (2013), pp. 24–29.
- [57] Grant Ingram. “Basic Concepts in Turbomachinery”. In: (2009).

- [58] Siemens®. *Solid Edge 2019*. Version 2019. URL: <Https://solidedge.siemens.com>.
- [59] M. Beiler and T. Carolus. “Computation and measurement of the flow in axial flow fans with skewed blades”. In: *American Society of Mechanical Engineers Journal of Turbomachinery* 12 (1999), pp. 59–66.
- [60] ANSYS®. ANSYS. Version 17.1. 2016. URL: <https://www.ansys.com>.
- [61] R. Engel, C. Silva, and C. Deschamps. “Application of RANS-based Method to Predict Acoustic Noise of Chevron Nozzles”. In: *Applied Acoustics* 79 (2013), pp. 153–163.
- [62] M. Gennaro et al. “Zonal Large Eddy Simulation for Numerical Prediction of the Acoustic Performance of an Axial Fan”. In: *6th European Congress on Computational Methods in Applied Sciences and Engineering* (2012).
- [63] M. Shur et al. “A Rapid and Accurate Switch from RANS to LES in Boundary Layers Using an Overlap Region”. In: *Flow Turbulence and Combustion* 86 (2011), pp. 179–206.
- [64] ANSYS®. “ANSYS Fluent User’s Guide”. In: (2013).
- [65] S. Proskurov, O. Darbyshire, and S. Karabasov. “Aerofoil broadband and tonal noise modelling using stochastic sound sources and incorporated large scale fluctuations”. In: (unknown).
- [66] Cambridge University. “Materials Data Book”. In: (2003).
- [67] Roger George®. “Roger George Special Effects”. In: (2019). URL: <https://rogergeorge.com/collections/fans-wind>.
- [68] P. Spalart and M. Shur. “Variants of the Ffowcs Williams - Hawkings Equations and their Coupling with Simulations of Hot Jets”. In: *International Journal of Aeroacoustics* 5 (2009).
- [69] A. Zinoviev. “Application of Ffowcs Williams and Hawkings Equation to Sound Radiation By Vibrating Solid Objects in a Viscous Fluid: Inconsistencies and the Correct Solution”. In: *Innovation in Acoustics and Vibration Annual Conference of the Australian Acoustical Society* (2002).
- [70] Aerovent. “Air Moving Equipment: Full Line Catalog”. In: (2013).
- [71] TEC. “Products: 2.2kw, 4 pole, foot and face mounted compact motor B34 IE2”. In: (2019).
- [72] C. Burgess and R. Thompson. “Practical Consideration of Noise from Fans”. In: (2014).

Appendix A

Motor Power

A.1 Initial Euler Equation of Turbomachinery

This calculation was conducted to ensure that the goal wind speed was realistic for a machine of the required size and power input.

From the fan efficiency equation, eq.3.7, the Power input needed is,

$$P = \frac{Q\partial p_t}{\eta} \quad (\text{A.1})$$

From Bernoulli's Equation, or the equation of transmission of shaft work to the fluid, eq. 3.6,

$$\partial p_t = \partial p_s + \frac{1}{2}\rho(c_2^2 - c_1^2) \quad (\text{A.2})$$

Taking the Static pressure change $\partial p_s = 10Pa$ from literature, and performance curves of similar fans [49], the inlet velocity, $c_1 = 5.08m/s$, density of air, $/rho = 1.225kg/m^3$, and required outlet velocity, $c_2 = 40mph = 17.88m/s$.

Then the total pressure rise is,

$$\partial p_t = 10 + \frac{1}{2}(1.225)(17.88^2 - 5.08^2) = 190Pa$$

The volumetric flow rate,

$$Q = Av = \frac{\pi}{4}(600 \times 10^{-3})^2 \times 17.88 = 5.055 \quad (\text{A.3})$$

Given a motor efficiency of 78.9% and estimating the fan efficiency to be 65%. Then,

$$P = \frac{190 \times 5.055}{0.789 \times 0.65} = 1.9kW \quad (\text{A.4})$$

The motor has an output power of 2.2kW. Therefore, theoretically the machine is of adequate size and power to supply the required winds, this was checked in accordance with the performance curves to ensure the power is still adequate when taking into account pressure losses. The impeller requires a power input of 1.3 kW so the motor power is adequate.

Appendix B

Performance Curves

B.1 Number of Blades PAG

These performance curves (Figure B.1) are for 5, 9 and 12 blades of the PAG M-blade propeller. The specifications are outlined in Table B.1. The 9-bladed impeller provides a balance between higher flow rate output, efficiency, and noise.

Number of Blades	5	9	12
Identifying number on curve	1	2	3
Efficiency [%]	60.8	58.7	45.28
$Q [m^3/s]$	3.489	3.644	3.711
Shaft Power [kW]	0.968	1.312	2.024
Noise Power [dB(A)]	81.47	85.4	88.91

Table B.1: Specification of Impellers [50]

B.2 Angle of Blades

Table B.2 demonstrates the different efficiencies, flow rates and power level of various blade pitch angles.

Angle of Blade [°]	32.5	35	37.5	45
Efficiency[%]	48.42	51.7	53.5	58.7
$Q [m^3/s]$	3.644	3.929	4.167	4.876
Shaft Power[kW]	0.9687	1.058	1.138	1.312
Noise Power[dB(A)]	87.62	88.55	89.45	92.45

Table B.2: Specification of Impeller with Different Blade Angles [50]

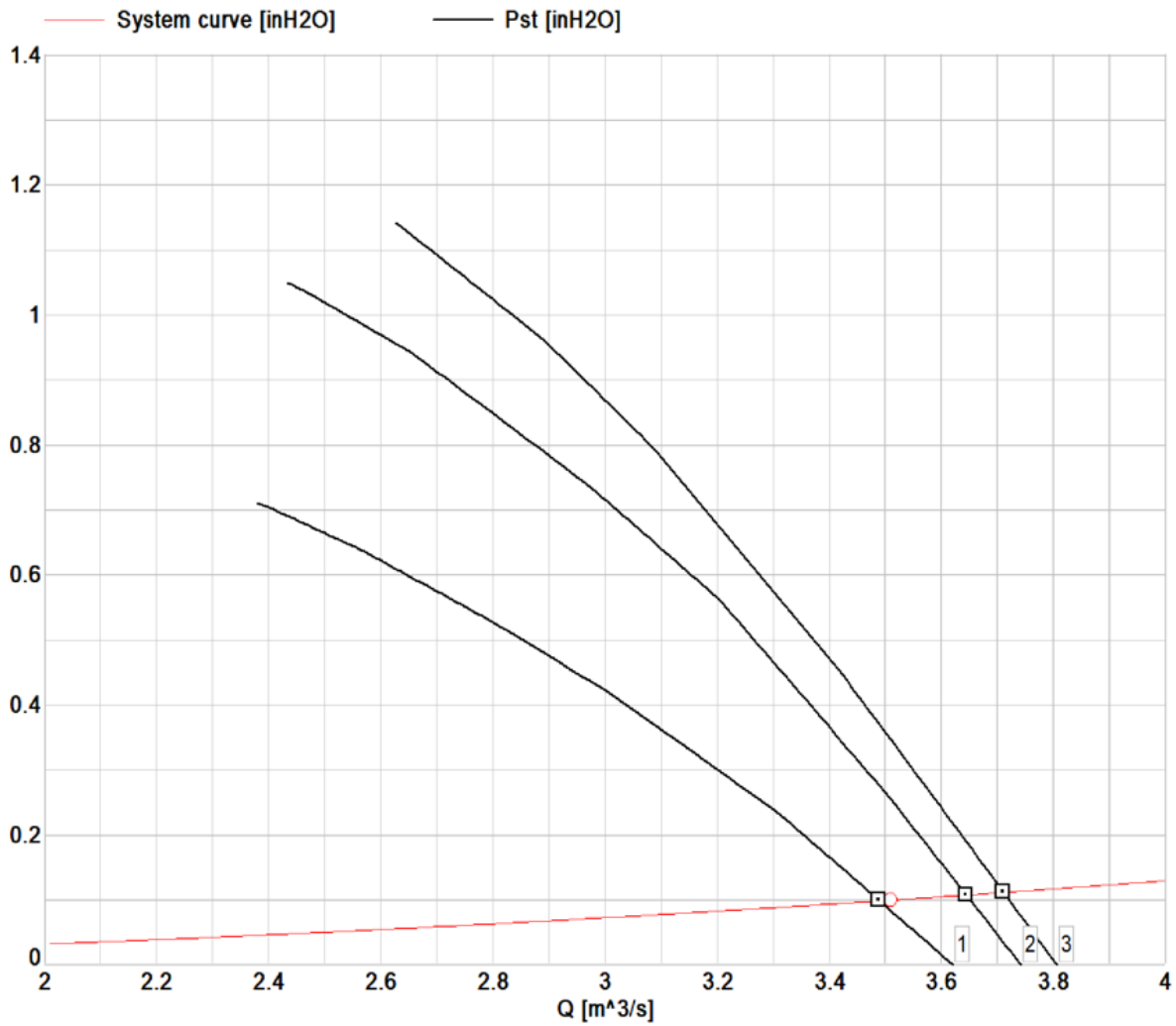


Figure B.1: Performance curves for PAG impeller with 5, 9 and 12 blades [50]

Appendix C

Stator

C.1 Flow Vectors for Stator Profile

Taking a mean-line approach to the blade, shown in Figure C.1

Assuming complete blade congruence of the flow from the rotor, which is a very crude assumption, take $\alpha_2 = 0$. This means that the relative flow is at $\beta_2 = 45^\circ$. The flow should be turned so that it is axially aligned. In reality, this will not happen completely but the stators should smooth the flow and direct it back towards the axial direction, i.e. $\beta_3 = 0$. This means that the angle of curvature, $\theta = 135^\circ$.

This can be approximated, for manufacturing purposes, as an arc turned through an eighth of a circle, or $\frac{\pi}{4} \text{ rad}$, with radius 113mm. This would produce an arc of chord length 86.5mm. A straight section should also be included in order to steady the flow and increase the turning effects. This will be 50mm long, producing a stator with 136.5mm chord length.

C.2 Blade Dimensions

The stators will be 3mm wide, which enables sufficient width and easy manufacturing of GRP.

The stators will be 612mm in length of their working face, but will be produced to be 24mm longer than this for attachment to the fan housing.

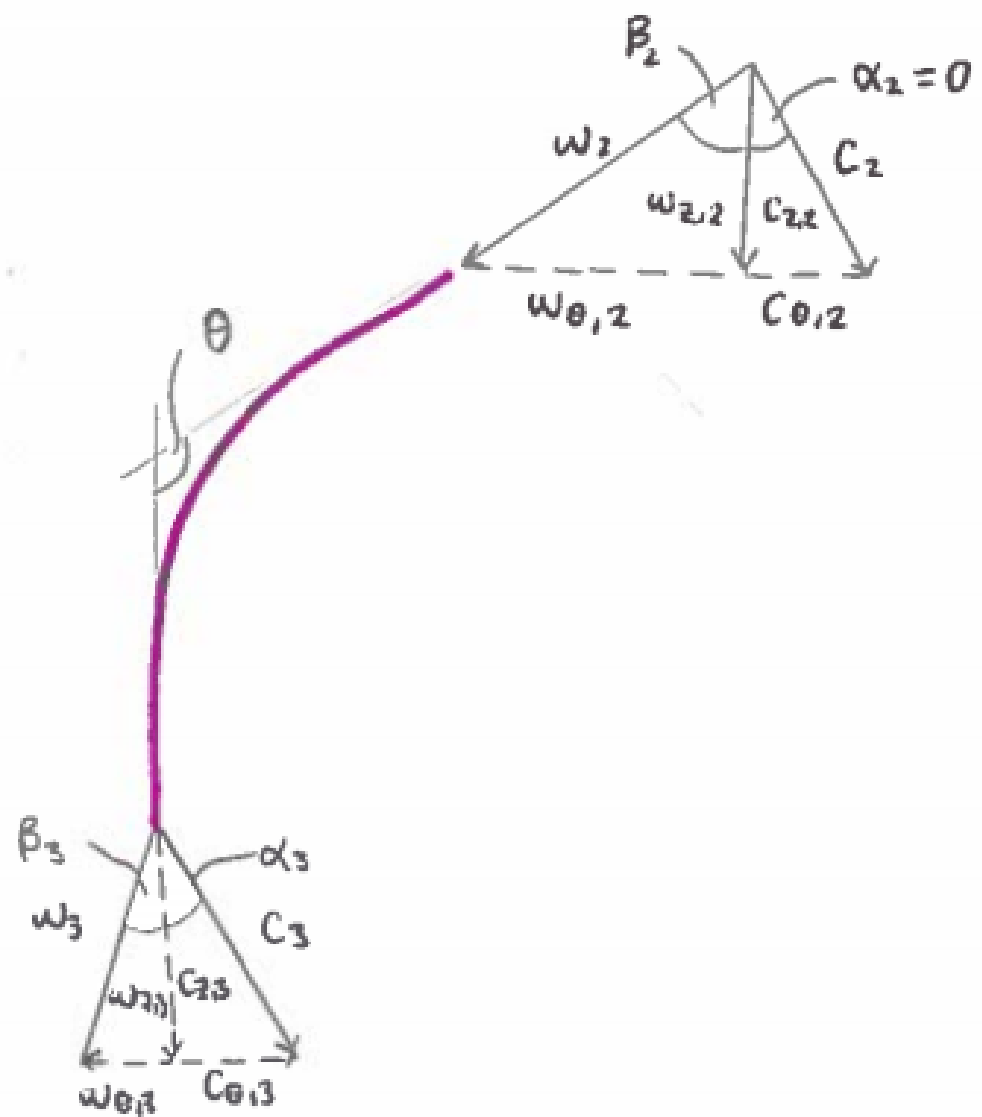


Figure C.1: Mean-line Flow Schematic with Velocity Vectors

Appendix D

Bolts

D.1 Stand Bolts

The diagram of the bolt and stand configuration is shown in Figure D.1. The purpose of bolt calculations is to determine the forces on the and the corresponding bolt size which can accommodate these loads.

The force on the bolt, F_{max} ,

$$F_{max} = F_a + \frac{F_t}{\delta} = \frac{2(60g)}{0.7} = 1681.71N \quad (\text{D.1})$$

where δ is the friction factor of steel-on-steel = 0.7, and F_t is the total force which is the weight of the structure (60g) multiplied by a Safety Factor of 2.

The average shear force on the bolt,

$$\tau_{shear} = \frac{F_{max}}{A_s} \quad (\text{D.2})$$

where A_s is the shear area, defined by,

$$A_s = \frac{\pi d^2}{4} \quad (\text{D.3})$$

where d is the nominal diameter of the bolt. For an M10 bolt this is 8.8.

The average bearing stress is then,

$$\tau_{shear} = \frac{1682}{60.82} = 27.66MPa$$

The Yield Strength of mild steel is approximately 370 MPa, and a standard safety factor of 0.6 is normally applied.

$$0.6(370) = 222MPa$$

This leaves a remaining safety factor of

$$\frac{222}{27.66} = 8$$

This allows for the dynamic stresses from any vibration occurring in the system and justifies the use of M10 bolts.

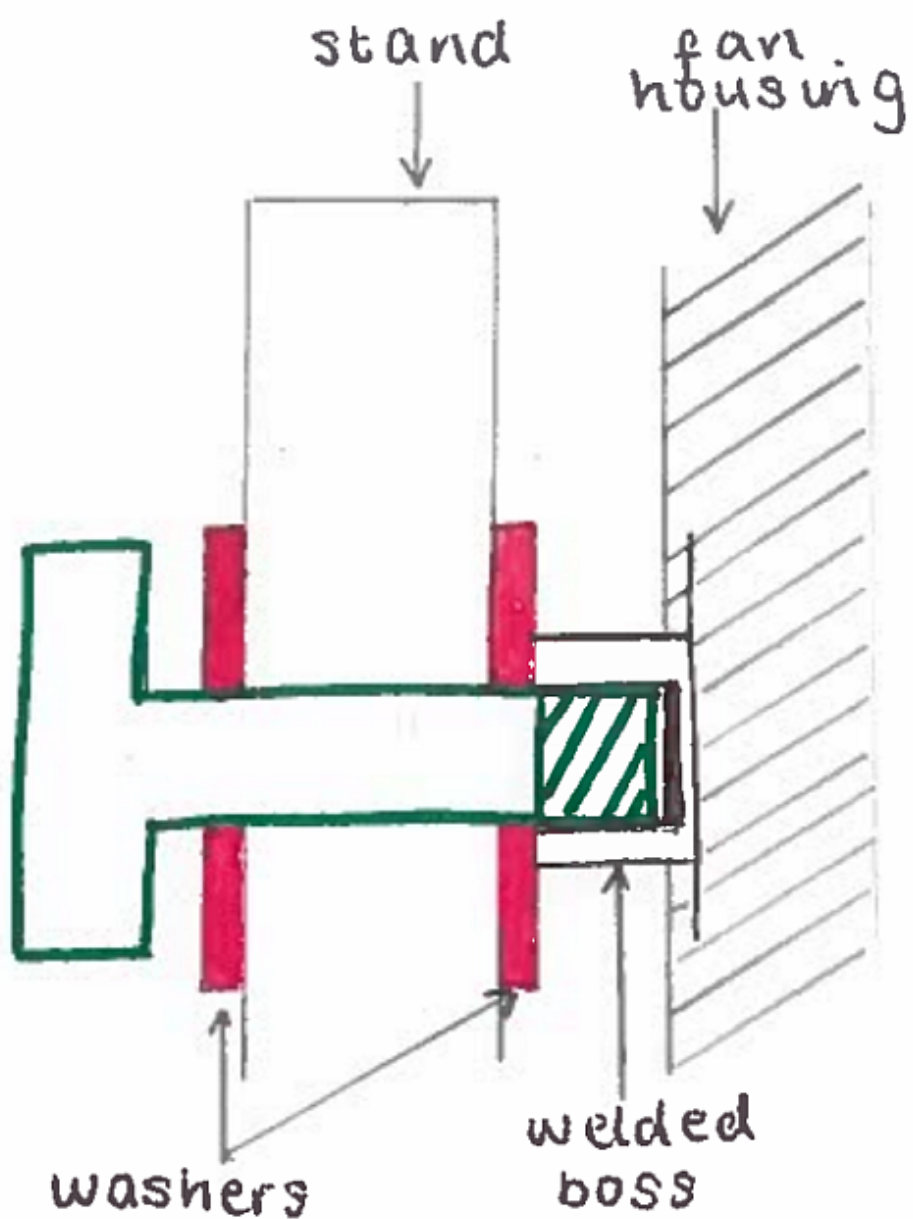


Figure D.1: Schematic of Bolt Configuration for U-stand and Fan Housing Interface

Appendix E

Static Balance

The housing was approximated as a beam simply supported at some point, A, with the forces of the various loads applied to it. The forces are assumed to be point forces acting at their centre of gravity. This is shown in Figure E.1.

Taking moments about A,

$$11g(A + 100) + 18g(A - 140) - 20g(27.5 - A) - 2g(342.5 - A) - 2g(480 - A) = 0$$

$$A(11g + 18g + 20g + 4g) = 8565g$$

$$A = \frac{8565}{53} = 161.6mm$$

For simplicity, A will be placed at 160mm from the housing entrance, not including the bell inlet. This will mean that the fixture is very close to the centre of mass of the motor. This is the heaviest component so this is intuitively correct.

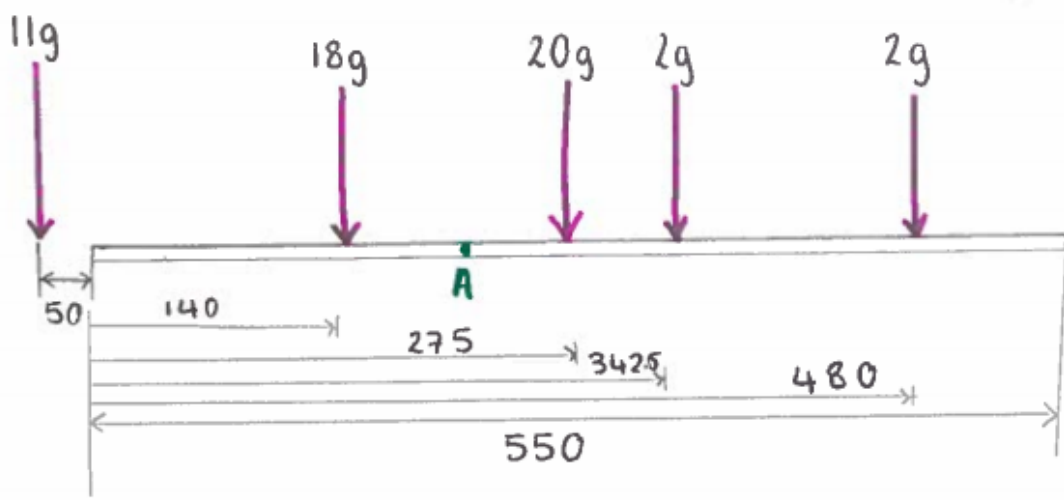


Figure E.1: Free Body Diagram for Static Balance of Components in Fan Housing

Appendix F

U-Stand Loading

The U-Stand was approximated as an eccentric axial loaded column, see Figure F.1.

Where $e = 34\text{mm}$ due to the 30mm length boss and 8mm thickness stand. The force through the structure is,

$$P = \frac{1}{2}(Mg) = 30(9.81) = 294.3$$

The bending stress,

$$\sigma_b = \frac{Mc}{I}$$

where I is the moment of Inertia defined by $I = \frac{b}{12h^3} = 1.365 \times 10^{-9}\text{kg.m}^2$, and c is the position of the neutral axis relative to the centroid of the cross section, $c = 1.3\text{mm}$. This gives $\sigma_b = 38.12\text{MPa}$

The axial stress, σ_a is given by,

$$\sigma_a = \frac{P}{A} = 1.14\text{MPa}$$

This means that the total stress $\sigma = 39.26\text{MPa}$. Compared to a yield stress of steel of $\sigma = 250\text{MPa}$, this gives a safety factor of 6.36 which is adequate to allow for the dynamic loading of the system.

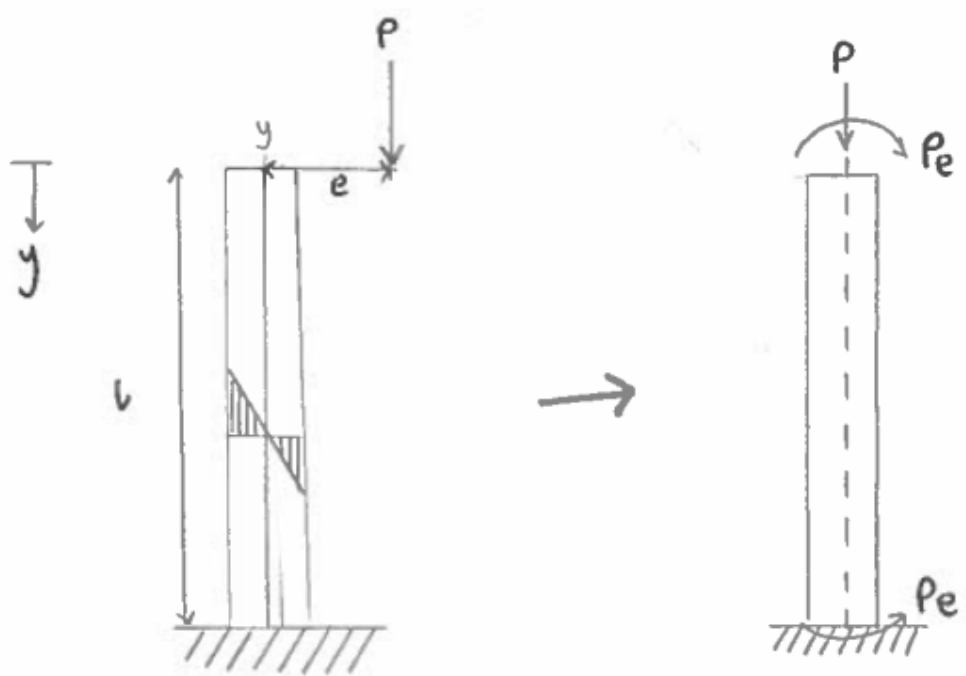


Figure F.1: Free Body Diagram of U-Stand Loads

Appendix G

Project Planning

The original Gantt Chart is shown in Figure G.1, where the activity descriptions are given in Table G.1. This allowed for some float time in the design and manufacturing stages. Design delays occurred due to the sheer quantity of information processing required to gain a solid understanding of the theory in order to execute a rational design. From February, the design process accelerated with the final design presented 8 days later than originally expected. This was allowable in the original float time for the project. However, further significant delays occurred with material ordering and manufacture. This meant that the final machine could not be tested in time. However, most of the objectives of the project were achieved regardless.

Task Name	Task(letter)	Start Date	Predicted Duration [Days]	Predicted End Date	Actual End Date
Background/Project Brief	A	15-Jan	9	24-Jan	15-Feb
Impeller/motor calcs.	B	15-Jan	9	24-Jan	24-Jan
Interim Report	C	28-Jan	17	14-Feb	14-Feb
Impeller/stator/cowl design	D	24-Jan	14	07-Feb	20-Feb
Optimisation of Design	E	04-Feb	6	10-Feb	25-Feb
Casing and Stand Design	F	10-Feb	5	15-Feb	27-Feb
CAD Modelling	G	12-Feb	3	15-Feb	28-Feb
Optimisation of Design	H	15-Feb	7	22-Feb	03-March
Presentation of Design	I	17-Feb	5	22-Feb	03-March
Material Orders	J	11-March	14	25-March	20-April
Construction	K	25-March	14	10-April	ongoing
Testing	L	10-April	7	17-April	N/A
Report Write-up	M	22-Feb	60	23-April	29-April
Presentation	L	23-April	31	24-May	24-May

Table G.1: Task Definition for Gantt Chart

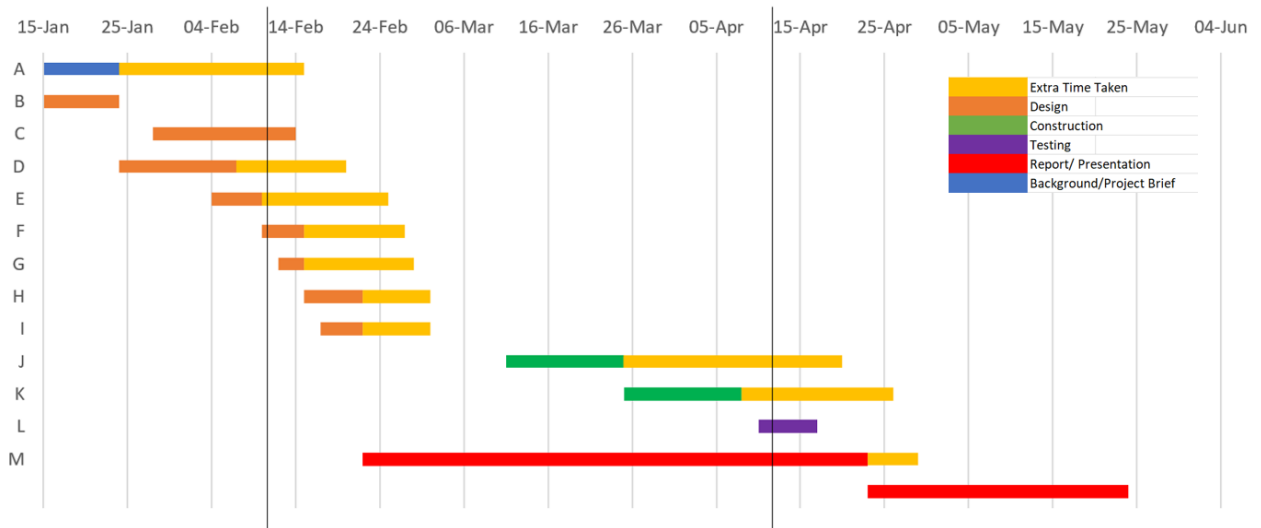


Figure G.1: Gantt chart used for project planning compared to the actual time taken for the activities